Industrial Technology and Analysis of GaAs

NOUBAR YEMENIDJIAN

A Thesis

in

The Faculty

of

Engineering and Computer Science

Presented in Partial Fulfillment of the Requirements
for the Degree of Doctor of Philosophy at
Concordia University
Montreal, Canada
October, 1982

© NOUBAR YEMENIDJIAN, 1982

ACKNOWLEDGMENT

I would like to thank my supervisor, Dr. B.A. Lombos for his help in the experimental as well as theoretical suggestions and discussions during the entire duration of this experiment, as well as his moral support and encouragement.

I also would like to thank the present and former Deans of Engineering at Concordia University, Dr. M.N.S. Swamy and Mr. J.C. Callaghan for their continuous encouragement and financial support for the entire duration of this research, and last but not least, I would like to thank the machine shop personnel for their cooperation in the design and machining of many of the components of the experimental apparatus.

ABSTRACT

Industrial Technology and Analysis
of GaAs

Noubar Yemenidjian, Ph.D.
Concordia University, 1982

A heat pipe assisted zone melting furnace for the synthesis and single crystal growth of large (up to 55 mm) diameter GaAs is described.

The high thermal conductivity of the heat pipe and the dynamic profile design makes possible the precise control of the background temperature, hence the arsenic vapour pressure. Because of the well defined narrow molten zone, the number of impurities were few and their concentrations minimized.

A multilevel model was developed to calculate the position of the Fermi level in GaAs. All the electrically-active impurity concentrations, indicated by spark source mass spectrographic analysis, were taken into account in the computation. The deduced semiconducting or semi-insulating properties are in agreement with the measured characteristics of the investigated crystals. It is shown that, in the case of the large gap semiconductors, only deep-lying compensation results in high resistivity, semi-insulating materials.

TABLE OF CONTENTS

			Page
CHAPTER 1		INTRODUCTION	1
CHAPTER 2		REVIEW OF GROWTH METHODS AND TRANSPORT PROPERTIES	4
	2.1	Characterization	17
	2.2	Semi-insulating Gallium Arsenide	22
	2.3	Imperfection-associated energy levels in Gallium Arsenide	22
CHAPTER 3		CRYSTAL GROWTH	27
	3.1	GaAs Crystal Growth by Zone Melting	27
	3.2	Heating Arrangement	32
	3.3	Principle and Characteristics of Heat Pipes	33
	3.4	Heat Pipe Construction	38
	3.5	Heating Element Considerations	43
	3.6	New Heating Element and Furnace Design	48
	3.7	Final Design; Dynamic Temperature Profile	51
	3.8	Nucleation Control	55
	3.9	Ampule Preparation	58
CHAPTER 4		CHARACTERIZATION	60
	4.1	Analyses	68
	4.2	Results and Discussion	74

CHAPTER 5 SUMMARY AND CONCLUSION.......................... 88

REFERENCES... 90

APPENDIX A 95

LIST OF ILLUSTRATIONS

Figure		Page
2.1	Segregation Profile in Normal Freezing (BRIDGMAN) or LEC	12
2.2	Zone Melting Model	15
2.3	Segregation Profile in Zone Melting	15
2.4	Distribution Coefficient $K_s = C_s/C_l$ of Impurities in GaAs as a Function of Ionic Radius	19
2.5	Diffusion Coefficients in GaAs at Low Concentration Limit	20
2.6	Summary of Imperfection Energy Levels, eV, in Gallium Arsenide	24
3.1	Desired Temperature of Zone Melting Furnace	31
3.2	Initial Furnace Design	34
3.3	Theoretical Working Fluid Heat Transfer Capability	40
3.4	Cross-sectional View of Heat Pipe	44
3.5	Furnace Temperature Profile	45
3.6	KANTHAL A1 Strip Heater	49
3.7	Final Furnace Temperature Profile	52
3.8	Circuit Diagram Furnace Control System	54
3.9	Double Tip Boat	57
4.1	A Crystal Grown by Zone Melting	61
4.2	Typical Dislocation Densities in GaAs	63
4.3	Hall Sample Dimensions	66
4.4	Measurement Arrangement	67

4.5 Carrier Concentration Versus Energy
Sample No. 1............................ 82

4.6 Sample No. 2............................ 83

4.7 Sample No. 3............................ 84

4.8 Sample No. 4............................ 85

4.9 Sample No. 5............................ 86

4.10 Typical Curves of $\ln(R_H\, eT^{3/2})^{-1}$ as the Function Reciprocal Temperature of Semi-insulating GaAs Samples Based on the Measured Data Collected in Table 4.3..... 87

LIST OF TABLES

Number		Page
2.1	Typical Impurities of Fused Silica........	21
3.1	Physical and Mechanical Properties - 300 Series Stainless Steels..................	39
3.2	Selected Working Fluid Characteristics....	41
4.1	Spark Source Mass Spectrographic Analyses of GaAs Samples 1 to 5, for trace Impurities, the Concentrations are Semiquantitative..........................	62
4.2	The Measured (Me) and Calculated (Ca) Hall Coefficients (R_H), Electron (n), Hole (p) Concentrations, Mobilities (μ_H), and Resistivities (ρ) of Samples 1 to 5....................................	75
4.3	Results of Hall Effect Measurements of Cr Doped Semi-insulating GaAs, Samples 2,7 and 8..................................	81

CHAPTER 1

INTRODUCTION

As a result of several decades of experience, and ease of fabrication as well as low cost, present device technology is centered around silicon. But growing requirements for devices providing fast response and operation in high temperature, high power, high frequency and low noise range, as well as need for optoelectric devices, make semiconductors with large direct band gap and high electron mobility most attractive. One of the best known semiconductors that satisfies the above conditions is Gallium Arsenide (GaAs).

GaAs is a compound semiconductor, consisting of group III element Gallium and group V element Arsenic. It has a direct band gap of 1.43 eV at room temperature (300°K) (1.1); forms solid solution with other III - V compounds to provide a wide range of band gaps. Its resistivities can range from less than 10^{-4} to as high as $10^{+8}\Omega$ - cm, making it suitable for direct active device fabrication. High resistivity substrates are suitable for epitaxial layers since they do not need to be isolated by p-n junctions as in the case of silicon integrated circuits. Some of the devices made from GaAs include Gunn diodes, laser diodes, photoconductive detectors, photocathode detectors, acoustic amplifiers, heterojunction photo cells and windows for CO_2 lasers.

Recent processing techniques have enabled the manufacture of high speed switching devices (up to 30 times faster than silicon). High

speed GaAs computer memory (4K bits) is commercially available and very large scale integrated circuits (VLSI) are being used in space applications.

As the applications of GaAs steadily increase, especially in devices such as lasers and high speed transistors, the need for improved crystalline perfection, as well as better understanding of the transport properties becomes essential.

From a crystalline point of view, the minimization of defects (dislocation) is difficult. In addition to the thermal inhomogeneities, due to the compound nature of GaAs, additional defects can be introduced by off stoichiometry growth. The toxicity and vapour state of the arsenic, during growth, requires containment and special handling procedures.

The large range of resistivities attainable in GaAs can be used advantageously. Chrome doping results in high resistivity material, but the outward diffusion of Cr into epitaxially grown active region might be undesirable. Therefore, the concentration of impurities and dopants should be kept to a minimum.

The scope of this study is the implementation of the zone melting technique to the growth of GaAs. It is believed that this technique combines many of the desirable features of the other methods, that is, the possibility of controlling the stoichiometry as in the Bridgman method, thereby improving the dislocation density, and similar to the liquid encapsulation technique in producing crystals of

high purity.

The narrow molten zone eliminates the sagging of the fused silica tube, and the need for elaborate support. Furthermore, it eliminates the deformation of the crucible and allows the growth of large diameter crystals.

Several crystals with and without doping have been grown by the zone melting technique. As expected, impurity diffusion from the boat and ampule are lower in concentration than those grown by the bridgman technique; whereas dislocation densities are generally lower than those grown by the LEC technique.

A multi level model is developed to determine the transport properties. Taking into account all the impurities indicated by the Spark Source Mass Spectrographic Analysis and their ionization potentials, the Fermi level is calculated from the charge neutrality condition. Subsequently the carrier concentrations, resistivity, and Hall coefficient are calculated.

The model takes into consideration the shallow and deep acceptors and donors as well as intrinsic carrier concentration. A computer program and a graphical method for the determination of the Fermi level are given in Appendix A.

CHAPTER 2

REVIEW OF GROWTH METHODS AND TRANSPORT PROPERTIES

GaAs is not as easy to grow as silicon and therefore its crystalline perfection as well as its purity does not yet match that of commercially available silicon.

GaAs is a compound semiconductor with a melting point of 1238°C. Gallium has a melting point of 29°C while arsenic sublimes and has a vapour pressure of 1 atmosphere at 613°C. Upon heating, GaAs dissociates and some arsenic is lost. During synthesis of the compound, to achieve stoichiometric composition and thermodynamic equilibrium, a vapour pressure of As of .973 atmospheres (dissociation pressure) is necessary. This pressure corresponds to 612°C. Therefore, to synthesize the compound under thermodynamic equilibrium, it is necessary to have a furnace with at least two temperature zones. One to heat the Gallium to 1238°C, and the other to control the minimum temperature of the system (612°C), so that the corresponding As pressure within the system is .973 atmospheres.

Gallium Arsenide crystal growth can be divided into two categories; one where the melt is in thermodynamic equilibrium, and the other where it is under non-equilibrium conditions. Growth techniques that are classified under the former are Bridgman (horizontal or vertical) (2.1), zone melting (2.2), and Gremmelmaier (2.3), and the latter is the modified Czochralski, commonly known as liquid encapsulation (LEC) (2.4).

For several decades Czochralski growth has been well adapted to silicon crystal growth and the technique has reached a high degree of perfection. Single crystals of up to 150 mm diameter, 1800 mm length with automatic diameter control and practically dislocation free are commercially grown. Therefore, because of its familiarity, the Czochralski method with some modification has been adapted to the growth of GaAs. Crystal sizes range from 50 to 75 mm diameter and 100 to 200 mm in length.

The principle of this method is as follows: for elemental semiconductors such as silicon or compound semiconductors with non-volatile elements, only one temperature zone is necessary. The crucible is placed in a sealed chamber. The chamber is kept under vacuum or filled with inert gas. The crucible is heated to a few degrees above the melting point of the crystal. A seed crystal attached to a rod (seed holder) is lowered into the melt, and after equilibrium conditions are established, the seed is slowly raised. To achieve thermal homogeneity, the growing crystal, and sometimes the crucible as well, should be rotated. Most parts of the grower as well as the shell are water cooled. Several windows on the shell enable visual inspection. This is necessary to ensure that proper seed contact has been achieved. Such a system cannot be used to grow GaAs because the volatile component is not contained, and the dissociation of this compound will result in the evaporating arsenic continuously condensing on the cold walls of the shell. To overcome this problem a very ingenious technique is used. After placing the gallium and arsenic in the crucible together with dopants (if necessary), the contents of the crucible are covered with

an encapsulant.

In order to enable the growth of dissociable compounds, the encapsulant should have the following properties: it should be fluid at a temperature where the sublimation of the volatile component is insignificant; it should wet the solid and liquid compound as well as the crucible; it should remain relatively viscous; it should be transparent; it should not contaminate the melt; and, should have a coefficient of thermal expansion similar to the crystal to be grown in order not to subject the grown crystal to stress.

The advantages of such a system is the unconstrained growth of the crystal, and the resulting round cross-section makes it very attractive from a device manufacturing point of view, as this makes possible the use of silicon processing equipment. Seeding is easier than other growth methods and the cross-section of the crystal is, in general, larger than those grown by other methods.

The most common encapsulant that satisfies most of the above-mentioned requirements is boric oxide (B_2O_3). Unfortunately, there are some drawbacks to this system. There is some degree of contamination from the encapsulant, in addition, B_2O_3 is hygroscopic and has to be heated under vacuum at high temperatures (above 1000°C) for over 24 hours (in a platinum crucible) to remove all traces of moisture; otherwise it hinders the view and severely contaminates the melt. From the beginning of growth, the full charge is molten and the ungrown portion of the charge is continuously exposed to temperatures exceeding the melting point of the compound. This results in a large volume and long time exposure of the liquid to the surrounding crucible and

encapsulant, thereby increasing the possibility of contamination; and, because the melt is covered with encapsulant, gas doping is not possible.

A more serious problem is the arsenic pressure in the system. As the full amount of arsenic is heated to above 1238°C, the vapour pressure of arsenic reaches over 60 atmospheres (as compared to .937 atmospheres required for stoichiometric growth), and pressure balancing becomes necessary. The grown crystal which is also covered with the encapsulant has to be cleaned while hot; otherwise, because of the difference in coefficients of thermal expansion, the solidifying encapsulant cracks the surface of the crystal.

The above-mentioned difficulties refer to the technical obstacles, but there exists one more difficulty which affects the quality of the grown crystal. The softening point of B_2O_3 is such that some arsenic sublimes before the B_2O_3 is capable of encapsulating the charge, the loss of arsenic is not easily controllable and therefore cannot be compensated. As the melt is not in thermodynamic equilibrium, but is forcefully contained, stoichiometric growth becomes very difficult. The deficiency of arsenic can result in vacancies while excess arsenic, if intentionally added, can result in interstitial or substitutional arsenic atoms. This last drawback unfavourably affects the transport properties as well as the dislocation densities (2.5).

In systems where thermodynamic equilibrium exists, the Bridgman method is the one most widely used. The furnace consists of two temperature zones, one held at the melting point of the compound and the

other adjusted to control the dissociation pressure of the volatile component with a shallow gradient in between. The gallium is placed in a "boat"-shaped crucible. The boat and arsenic are placed in an ampule, and the ampule is sealed under vacuum (10^{-5} to 10^{-6} Torr). The amount of arsenic in the melt is proportional to the vapour pressure of arsenic, hence in principle, the stoichiometry can be achieved by precise control of the minimum (background) temperature in the system. In addition to stoichiometric amount required, excess arsenic is placed in the ampule to maintain the required vapour pressure. This excess amount condenses when the furnace is cooled down. The quality of the crystals in general is superior to LEC grown crystals, but drawbacks exist in this system as well.

In the Bridgman system, similar to the LEC system, at the beginning of growth the full amount of material is molten and the ungrown portion of the charge is continuously exposed to temperatures exceeding the melting point of the compound. This results in a large volume and long time exposure of the liquid to the surrounding boat and ampule environment increasing the possibility of contamination. Furthermore, in the case of GaAs growth, due to its high melting point, the fused silica tube used as the ampule has a tendency to sag, because the total length of the boat is exposed to temperatures above the softening range of the fused silica. This necessitates an elaborate support system. Usually, the support tube is made of Silicon Carbide (SiC) because of its good thermal shock resistance. The SiC tube is attached at both ends to vibration-free posts, independent of the furnace. The crystal remains stationary and the furnace travels. Large

diameter SiC tubes are not readily available and hence cause limitation in size of the crystals. The cross-section of the crystal is usually semi-circular and is not very suitable from a processing point of view. Because of the negative coefficient of thermal expansion of GaAs, it is not possible to grow round cross-section in a crucible even in a vertical system; but, in a horizontal system a trapezoidal, or commonly known as "loaf shape" cross-section is possible. At present, undesired impurity levels in GaAs grown by the Bridgman method are an order of magnitude higher than those grown by the LEC method.

In the Bridgman as well as the LEC type growth, since the volume of the melt is constantly diminishing, the doping concentration will be as follows (2.6): assuming that the growth rate is such that (1) diffusion in the solid is negligible, (2) diffusion in the liquid is complete, (3) the segregation coefficient K is constant, let the length of the crucible be L_o, let the length of the solid be L_s, let the length of the liquid be L_L, let the fraction of the original value which has frozen be g, let the concentration of the dopant in the solid be C_s, let the concentration of the dopant in the liquid be C_L, let the original concentration be C_o, then

$$L_o = L_s + L_L \qquad K = \frac{C_s}{C_L} \qquad g = \frac{L_s}{L_o}$$

$$\int_0^{L_s} C_s dL_s = \text{the total amount of dopant in the solid at any instant}$$

C_oL_o = the total amount of dopant

$C_LL_L = C_oL_o - \int_0^{L_s} C_s dL_s$ = the total amount of dopant in the liquid at any time.

therefore,

$$C_L = \frac{C_oL_o - \int_0^{L_s} C_s dL_s}{L_L}$$

$$K = \frac{C_s}{C_L} = \frac{C_sL_L}{C_oL_o - \int_0^{L_s} C_s dL_s}$$

$$= \frac{C_s(L_o - L_s)}{C_oL_o - \int_0^{L_s} C_s dL_s}$$

hence $K[C_oL_o - \int_0^{L_s} C_s dL_s] = C_s(L_o - L_s)$,

differentiating

$$-KC_s dL_s = (L_o - L_s) dC_s - C_s dL_s$$

rearranging

$$C_s(1-K)\, dL_s = (L_o - L_s) dC_s$$

or $\int \frac{dL_s}{(L_o - L_s)} = \int \frac{dC_s}{(1-K)C_s}$

integrating $-\ln(L_o - L_s) = \frac{\ln C_s}{(1-K)} + M$ applying the boundary conditions

at $L_s = o$. $C_L = C_o$ hence $C_s = KC_o$

$$-\ln(L_o) = \frac{\ln K C_o}{(1-K)} + M$$

therefore,

$$M = -\ln(L_o) - \frac{\ln KC_o}{1-K} = \frac{(K-1)\ \ln(L_o) - \ln KC}{1-K}$$

$$= -\ln(L_o) - \frac{1}{1-K}\ \ln K C_o$$

hence
$$-\ln(L_o - L_s) = \frac{\ln C_s}{1-K} - \ln(L_o) - \frac{1}{1-K}\ \ln KC_o$$

$$\frac{\ln C_s}{1-K} = \ln(L_o) + \frac{1}{1-K}\ln KC_o - \ln(L_o - L_s)$$

$$\frac{1}{1-K}\ln\frac{C_s}{KC_o} = \ln\frac{L_o}{L_o - L_s}$$

$$\ln\frac{C_s}{KC_o} = (K-1)\ \ln\frac{L_o - L_s}{L_o}$$

$$= (K-1)\ \ln\ (1-g)$$

therefore,

$$C_s = KC_o(1-g)^{K-1}$$

Although, strictly speaking, the segregation coefficient does not remain constant. In practice, however, with growth rates of several centimeters per hour coupled with convection currents in the melt (due to thermal inhomogeneities), the basic assumptions remain

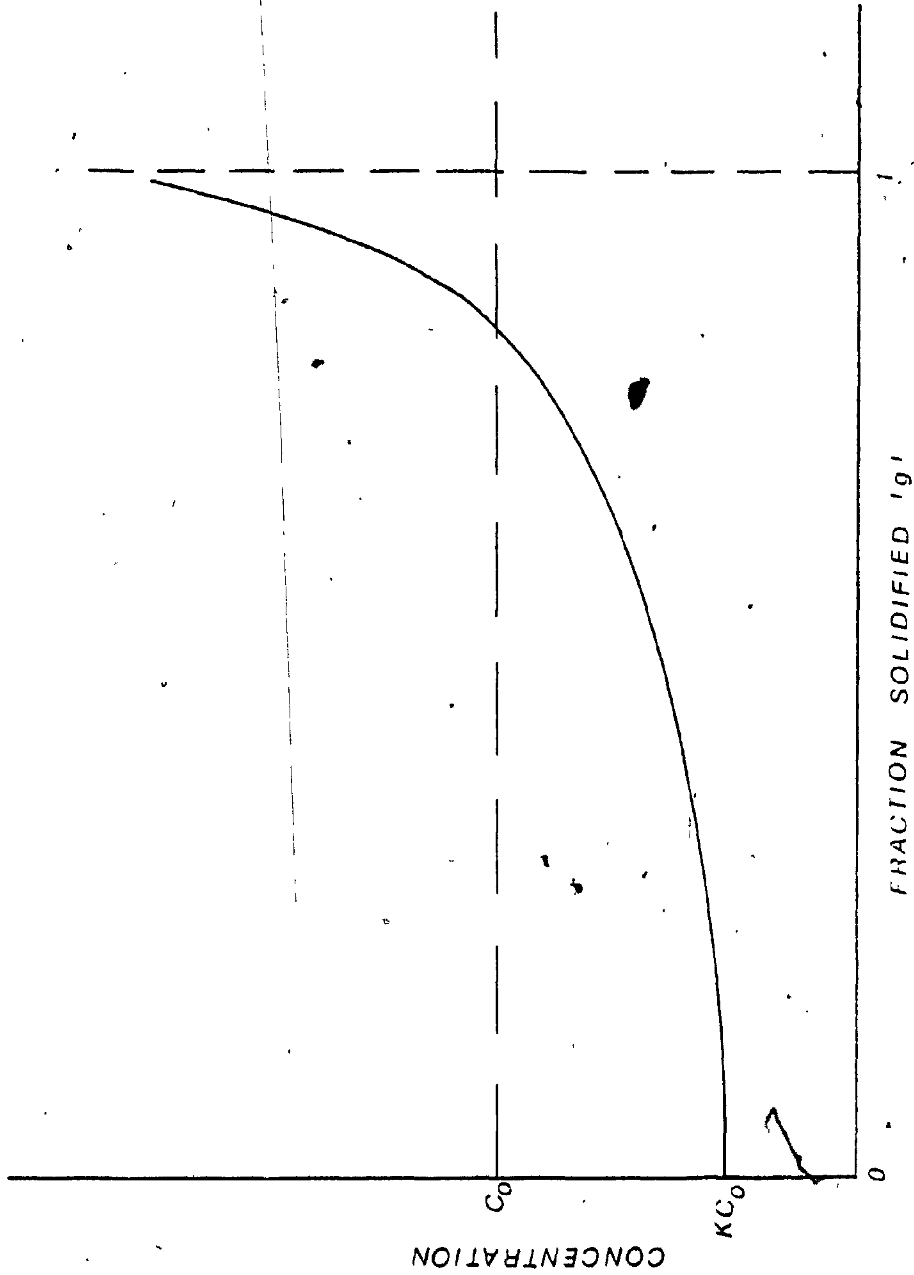

Fig. 2.1 Segregation profile in normal freezing (Bridgman) or LEC

valid. The resulting doping distribution is shown in Figure 2.1.

The Gremmelmaier method (2.7) is a combination of the original Czochralski and vertical Bridgman methods. The full charge is molten; the system is in thermodynamic equilibrium; the crucible and a magnetic seed holder (encapsulated in fused silica) are sealed in the ampule. To maintain the thermodynamic equilibrium, the minimum temperature of the system (including the magnetic material) should be maintained at 612°C (for GaAs). The crystal is pulled from the melt by applying an external magnetic field to the seed holder. Due to the severe limitation of high temperature magnetic materials and the complexity of the apparatus, this system is no longer in use.

Zone melting (2.6) is a relatively new method, it can be used for refining as well as single crystal growth and can be implemented in vertical or horizontal systems. Specifically applied to GaAs, the system is very similar to the classical Bridgman technique with the exception that only a narrow zone is kept molten at any one time. The melt is in thermodynamic equilibrium and to realize such a system a three zone furnace is necessary.

Applying principles similar to those in the Bridgman method the doping concentration as a function of length in the zone refining method can be derived as follows (2.6):

let C_o = mean concentration of solute in the charge, assumed to be invariant with x and expressed in units of solute per unit volume of solution.

K = distribution coefficient

L = length of molten zone.

C_x = concentration in freezing solid at distance x.

s = quantity of solute in zone at any distance x.

s_o = quantity of solute in zone at $x = 0$.

Let the cross-sectional area be unity, neglecting the change in volume due to the coefficient of expansion. By advancing the zone a distance dx, a volume dx of the melt will solidify, and a volume dx of the solid will liquify as shown in Figure 2.2.

The quantity of solute frozen out is $KC_L dx$, where C_L is the solute concentration in the molten zone. For unity cross-section $C_L = s/L$ while the amount of solute entering the melt is $C_o dx$. The net change in s is therefore given by:

$$ds = (C_o - KC_L)\ dx$$

$$= (C_o - K\ s/L)\ dx$$

therefore, $ds/dx + (K/L)s = C_o$

$$se^{(K/L)x} - s_o = C_o \int_0^x e^{(K/L)x}\ dx$$

$$= C_o\ L/K\ (e^{(K/L)x} - 1)$$

but the original solute $s_o = C_o L$

hence $\quad s = [C_o L + C_o\ L/K\ (e^{(K/L)x} - 1)]\ e^{-(K/L)x}$

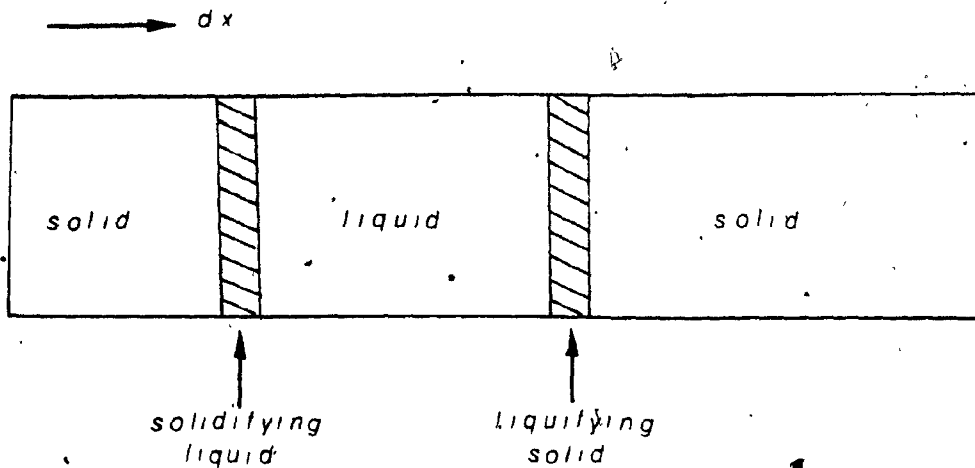

Fig. 2.2 Zone Melting Model

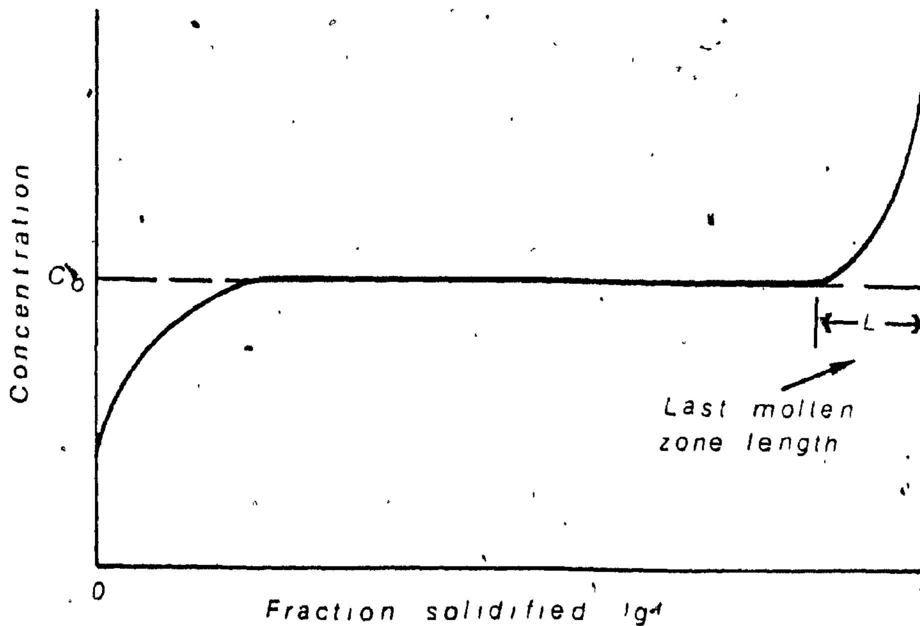

Fig. 2.3 Segregation profile in zone melting

$$= C_o L \left(\frac{K-1}{K}\right) e^{-(K/L)x} + C_o L/K$$

since $\quad C_x = KC_L = Ks/L$

hence $\quad C_x = C_o(K-1)e^{-(K/L)x} + C_o$

or $\quad C_x/C_o = 1 - (1-K)e^{-(K/L)x}$

The resulting doping concentration is shown in Figure 2.3. It can be seen that the concentration of dopants remains constant along most of the crystal length. Usually, the tip of the crystal is pointed, and gradually increases to the full cross-section. If this is made to coincide with the initial portion of the curve in Figure 2.3, then virtually all of the crystal length (of uniform cross-section) will practically be uniformly doped. Since in most cases the segregation coefficient is less than unity, the concentration of impurities in the last molten zone length will be very high and may even result in precipitation of dopants.

Another important feature of zone melting is the minimization of impurities diffused into the melt from the crucible. Since only a narrow zone is held at temperatures at or above the melting temperature, while the rest of the boat is kept at substantially lower temperatures; crystal purities higher than those achieved by the Bridgman method can be expected.

The combination of the best features of LEC growth (large

size) and Bridgman growth (thermodynamic equilibrium) can be achieved by zone melting. It should be noted that zone melting has its difficulties as well, such as maintaining steady state conditions in the presence of high temperature gradients, maintaining uniform growth rate, and possible nucleation problems. But with proper design considerations and correct interpretation of results, it should be possible to realize an adequate system.

2.1 Characterization

A survey of the literature on GaAs grown by various methods indicates that a large number of different impurity levels exist.. Because of the deep Fermi level of high resistivity GaAs, many deep impurity vacancy centers with concentrations much lower than those detected by chemical means, can be measured by thermally stimulated conductivity. Though electrical measurements do not indicate the type of impurities, knowing the different impurity energy levels, the impurities can be identified through their activation energies.

The sources of impurities are twofold. The impurities present in the starting materials and impurities introduced during the crystal growth. Both gallium and arsenic are available in 6'9 grade, meaning 99.9999% pure. Gallium is also available in 7'9 grade but its usefulness is questionable because during the handling minor contamination is unavoidable. The detectable impurities in gallium are (2.8), aluminum, silver, calcium and silicon. Impurities in arsenic are silicon, carbon, aluminum, calcium and sulphur. Since arsenic readily oxidizes, usually some oxygen is unintentionally

introduced.

In general, the concentration and distribution of impurity contaminants are determined by two factors: the distribution coefficient and the diffusion coefficient. Figure 2.4 shows the distribution coefficient of impurities in GaAs versus ionic radius (2.9) and the temperature dependence of diffusion coefficients in GaAs is shown in Figure 2.5 (2.10). It can be seen from Figure 2.4 that Na has a distribution coefficient greater than unity; hence, it appears only in the first grown portion of the ingots, provided that the source of contamination is in the starting material only. Unfortunately, triply ionized gallium interferes with sodium at M/e 23 so that traces of sodium cannot be determined by spark source mass spectrographic analyses (MSA).

In the case of Bridgman growth, the crucible as well as the ampule are additional sources of contamination. Typical impurity concentration in parts per million are given in Table 2.1.

Heating of fused silica to temperatures above 1350°C, causes the SiO_2 to undergo dissociation. This is generally considered to be $SiO_2 \xrightarrow[\Delta]{1350°C} SiO + 1/2\ O_2$ but even at lower temperatures some dissociation of fused silica takes place through the reaction $4Ga + SiO_2 \longrightarrow 2\ Ga_2O + Si$. In the case of LEC growth, depending on the type of crucible used (alumina, fused silica, graphite or Boron Nitride), together with boric oxide as an encapsulant, in addition to the above-mentioned impurities, boron and oxygen may also be found in the ingots. Once the impurities diffuse into the crystal,

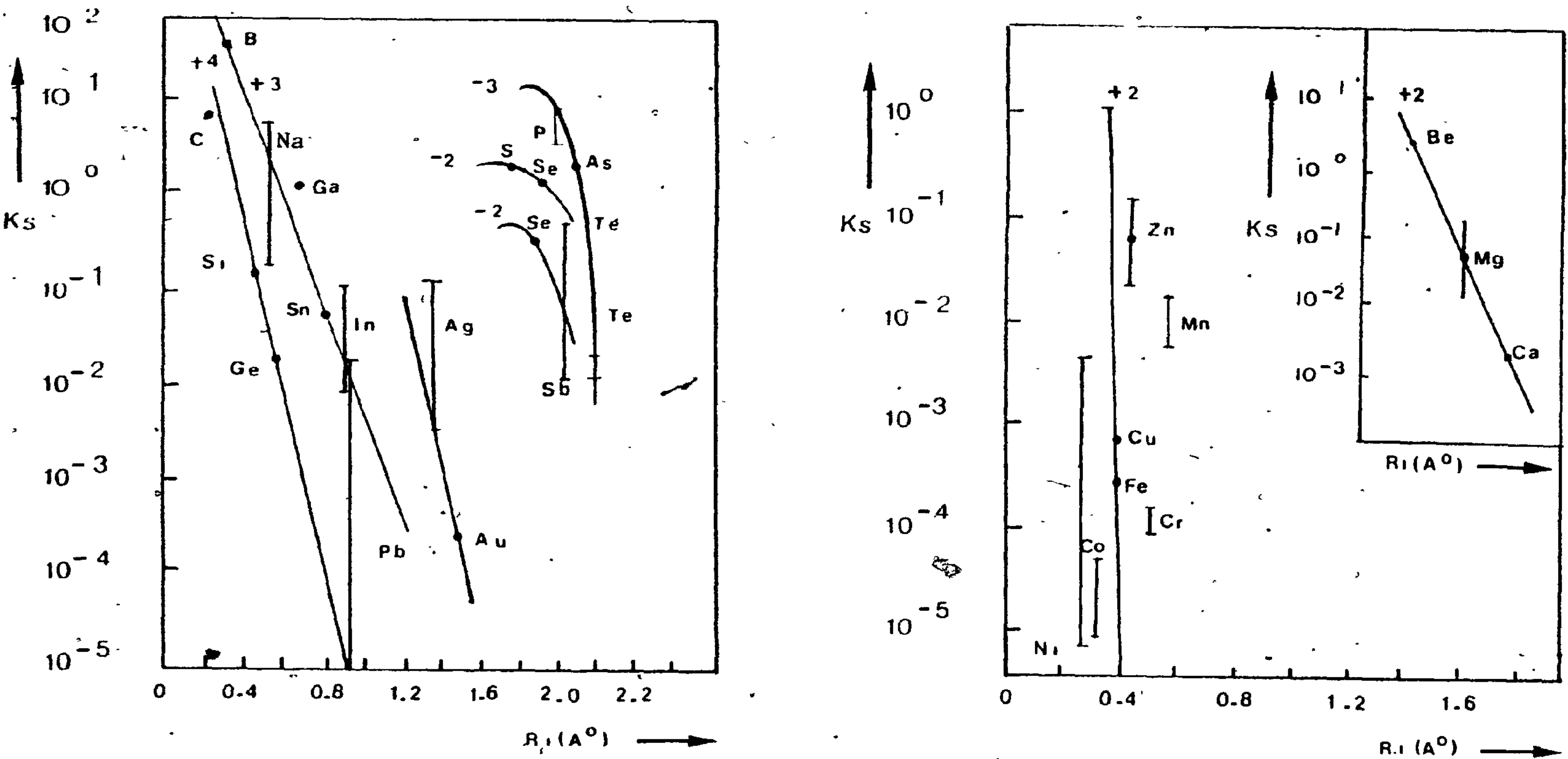

Fig. 2-4 Distribution Coefficient $K_S = C_S / C_L$ of impurities in GaAs as a function of ionic radius

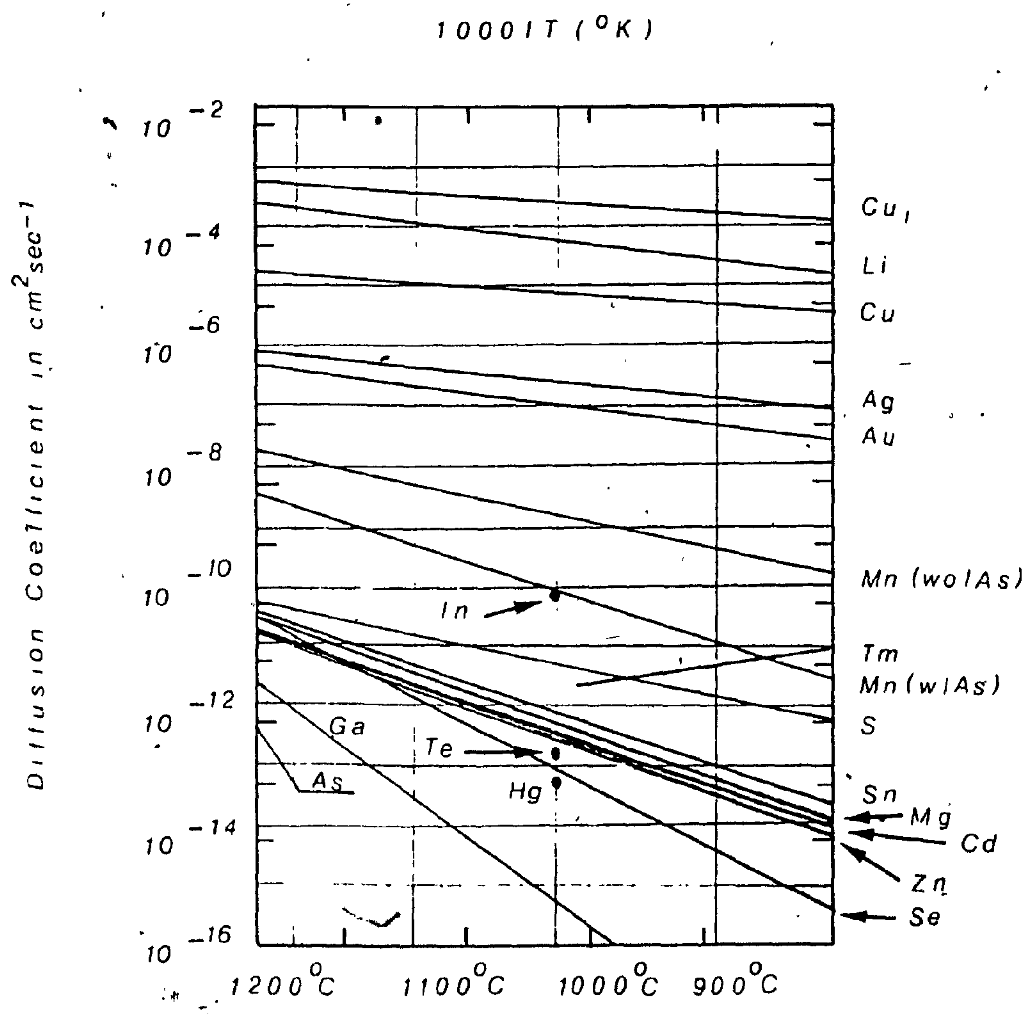

Fig. 2.5 Diffusion Coefficients in GaAs At Low Concentration Limit.

Table 2.1: Typical Impurities of Fused Silica (as supplied by General Electric Company, for type 204 tubing)

Elements	Concentrations (p.p.m.)
Aluminum	26
Boron	<1
Calcium	3
Chromium	1
Iron	3
Lithium	.5
Magnesium	2
Potassium	3
Sodium	3
Titanium	2
Zirconium	3
Copper	<1
Manganese	2

they can act as simple dopants or react with other impurities or native defects to form complexes, thus increasing the complexity of the material properties.

2.2 SI GaAs:

Two common methods (2.11) of producing semi-insulating GaAs are Cr or O_2 doping. Undoped crystals grown by the Bridgman technique are of low resistivity type. As a result of unintentional doping, semi-insulating crystals are grown by the LEC technique. Chemical analyses do not reveal the nature of the impurities associated with the deep levels, since chemical concentrations are not significantly different from those present in crystals grown by the Bridgman method. It is generally assumed that complexes are formed through the interaction of the melt with the B_2O_3 encapsulant introducing the deep lying compensation levels.

2.3 Imperfection-associated energy levels in GaAs:

A GaAs single crystal is a stoichiometric compound prepared from gallium and arsenic with different atomic radii and ionization potentials. As expected, an excess of one component over the other can lead to defects in the lattice. These in turn can behave as impurity levels. Because of such complicated environment, the energy levels due to impurities and levels resulting from off-stoichiometry in GaAs are not as easily predicted and controlled as in the case of pure covalent semiconductors. It is difficult to assign observed energy levels to definite centers in view of the large number of possibilities present in GaAs single crystals. In spite of much past work, only

some of the energy levels observed in GaAs are generally accepted to be due to specific centers. A great number of energy levels are still poorly understood. This situation may be caused by the interaction of one imperfection center with native defects and/or other impurities. Figure 2.6 shows the measured ionization energies for various impurities in GaAs. However, levels shown with broken lines are still not well understood. All levels above the gap center are measured from the bottom of the conduction band and are donor levels (except for those with broken lines). All levels below the gap center are measured from the top of the valence band and are acceptor levels, (except for those with broken lines and those marked D for donor levels), (2.8).

Figure 2.6 shows that the impurities of group IA, IB, IIA, and IIB of the periodic table are incorporated on Ga sites and are shallow acceptors. Although most of them diffuse into GaAs interstitially, only acceptor levels have been observed. Elements of Group IV are well known as amphoteric dopants in GaAs. Depending on the excess or deficiency of arsenic in the melt, both Si and Ge may occupy Ga or As sites respectively. Except for oxygen, the group VI elements such as S, Se, and Te tend to locate on As sites and introduce shallow donor levels. Oxygen is generally accepted as a deep donor in GaAs. Transition metals such as Fe, Co, Ni, Mn, etc., are found on Ga sites as deep acceptors (2.8).

Zinc is the most commonly used acceptor dopant, because it diffuses rapidly and has a large solid solubility. However, zinc diffuses anomalously, forms defects, and lowers the mobility; and thus device applications are limited. Germanium has been found to be an excellent

Fig. 2.6 Summary of Impurity Energy Levels, eV, in GaAs (2.8).

acceptor dopant, because the corresponding carrier lifetime is much higher. The most commonly used donor dopants are Se and Te. Also, Sn is used as a donor because of its low diffusion coefficient and low vapour pressure. This reduces cross-contamination around junctions.

It is well known that defects in crystalline materials can be classified into four categories: point defects, line defects, surface defects, and volume defects according to dimensionality. Because of improving crystal growth techniques for GaAs, single crystals free from surface and volume defects, except for precipitates of intentionally added dopants, are commercially available. The dislocation densities are in the range of 10^3 to $10^5/cm^2$, and usually of the LEC and Bridgman techniques, the latter yields lower dislocation densities.

From a device fabrication point of view, dislocation densities of presently available GaAs, as compared to silicon, are rather high. For this reason the approach has been to use bulk grown crystals as substrate material, and grow epitaxial layers for device fabrication. This requires that the substrate not participate in electrical conduction, hence the interest in high resistivity (SI) GaAs.

The most studied types of semi-insulating GaAs have been the oxygen doped or chrome doped types. Reported resistivities of chrome doped (in this study as well) have been as high as $5 \times 10^8 \Omega$-cm, while for oxygen doped 10^3 - $10^7 \Omega$-cm (2.8). Gas phase doping with oxygen is more difficult and less reproducible than chrome doping,

hence Cr doped material has become more common.

Considerable studies have been undertaken to characterize the properties of SI GaAs. Because of high resistivity, Hall effect measurements cannot be performed much below 0°C as the sample resistance becomes comparable to the input impedance of the electrometers. Photo Hall measurements can reveal more information at lower temperature and the energy levels of deep lying impurities can be found by optical absorption means as well (2.12).

Photoelectric properties of Cr doped high resistivity GaAs were reported by Lin et. al., (2.13). Deep level transient spectroscopy results were reported by Lang (2.14). Current-voltage characteristics (current oscillations) were reported by Kitahara et. al., (2.15). Two band model representing any two levels (impurity or otherwise) was proposed by Look (2.16) and Zucca (2.17), and a quasi four level model to calculate the Fermi level and relate the chemical impurity concentrations to the observed electrical properties was proposed by Linquist (2.18). The Fermi level in SI GaAs cannot be accurately calculated by taking into account one or two impurities only. A closed form expression for resistivity (ρ) and Hall mobility (μ_H) for more than two carriers is not developed yet. To date, common approaches have been to account for one or two shallow impurities (such as Si and/or C). Impurity concentrations indicated by MSA are "corrected" to yield best fitting curves (2.18).

CHAPTER 3

CRYSTAL GROWTH

3.1 GaAs Crystal Growth by Zone Melting:

As is discussed in the previous chapter, zone melting yields the most uniform doping and the least contamination from the boat and surrounding ampule atmosphere. Hence it was the chosen method of crystal growth. Though the advantages are evident, several difficult problems have to be overcome for the proper design of a zone melting furnace.

In principle single crystal growth consists of a stacking of atoms in a specific ordered structure. This requires that solidification start at a single point and proceed slowly unidirectionally. If the first nucleation is a single crystal and conditions are favourable, the growing crystal will also be single.

During the entire growth process, the growing solid is in contact with the remaining melt. At the solid-liquid interface, atoms from the melt continuously stack to the solid seed crystal. For successful growth it is desirable that the solid-liquid interface be smooth. This requires that the radial temperature distribution be very uniform.

Normally grains originating at a point on the solid-liquid interface grow perpendicular to the tangent at the point on the interface (3.1). This implies that if the interface is straight, grains will grow parallel to the growth direction. If the interface is concave with respect to the solid, grains will grow inwards and will

eventually criss-cross giving catastrophic results; or, if the interface is convex with respect to the solid, grains will grow outwards and eventually one single crystal can result. Due to the fact that even under best circumstances, some minimum wetting exists between the melt and the crucible, the most frequent origins of grains are the edges of the crystal. To ensure stable long single crystal growth, a slightly convex interface with respect to the solid is desirable.

The shape of the interface depends on the axial gradient within the crystal. If the gradient is large, the shape of the interface will be convex with respect to the solid. If the gradient is shallow, the interface will be concave with respect to the solid. Therefore, the temperature gradient of the furnace on the freezing side has to be adjusted in order to achieve a desirable solid-liquid interface shape.

In general, for all compound semiconductors, where at least one component is volatile, if the crystal is grown under thermodynamic equilibrium conditions, the stoichiometry of the compound will depend on the partial pressure of the volatile component. The pressure in the closed system is determined by the lowest temperature in the system. This requires that the minimum (background) temperature (controlling the pressure) in the system be known as well as maintained constant.

Fluctuations in background temperature induce changes in vapour pressure of the volatile component. This results in vacancies or excesses (interstitial or substitutional) of arsenic atoms in the crystal, and these in turn affect the dislocation density as well as

the transport properties.

In zone melting, only a narrow zone is maintained molten. Usually the molten zone length is one tenth the length of the crystal. This is achieved by having steep gradients on both sides of the narrow hot zone. Any small external disturbance such as a change in the ventilation may cause instabilities in temperature, which in turn induce fluctuations in growth rate. For this reason, the control of the hot zone temperature in a zone melting furnace, in general, is more difficult.

Figure 3.1 shows a desired axial temperature profile of a zone melting furnace. The hot zone temperature should be above the melting point of the crystal, to ensure that accidental freezing due to disturbances is avoided; yet, it should be as low as possible to minimize the diffusion of impurities from the surroundings. Practically, two degrees above the melting point is sufficient.

The gradient on both sides of the hot zone need not be symmetric; of these, the gradient on the freezing interface is much more critical as it will control the shape of the solid-liquid interface.

Assuming that the thermal conductivity of the crystal is constant, the total heat flow through the crystal will depend on the temperature gradient within the crystal. Since the heat source is thermal and not inductive, the core of the melt is slightly colder than the exterior. Furthermore, if the axial temperature gradient of

the crystal is large, its interior will be colder than the exterior. This will result in the center of the solid advancing into the liquid, hence a convex interface.

There are no strict requirements on the melting interface. In principle, to create a narrow zone as required for zone melting, a steep gradient is necessary; but, this in turn will increase the heat losses from the hot zone. This should be taken into consideration, in order not to exceed the power capacity of the hot zone heating element. A temperature gradient of 15-20°C per cm was found to be satisfactory.

The purpose of the background furnace is to control the minimum temperature in the system; hence, the partial pressure of the volatile component, maintaining it at the dissociation pressure of the compound. As the furnace travels and the relative position of the ampule changes, the minimum temperature of the system has to remain constant. This can be achieved in two ways: either the entire background furnace is kept at a constant temperature, or a thermocouple is placed at the end of the ampule and the temperature of the furnace controlled in order to maintain the end of the ampule at constant temperature. The former method is more difficult to achieve but yields better results.

The auxilliary furnace can serve two functions; first, by maintaining a temperature higher than the background temperature, it enables the background furnace to control the vapour pressure of the volatile component. Secondly, if the growth direction is from the hot

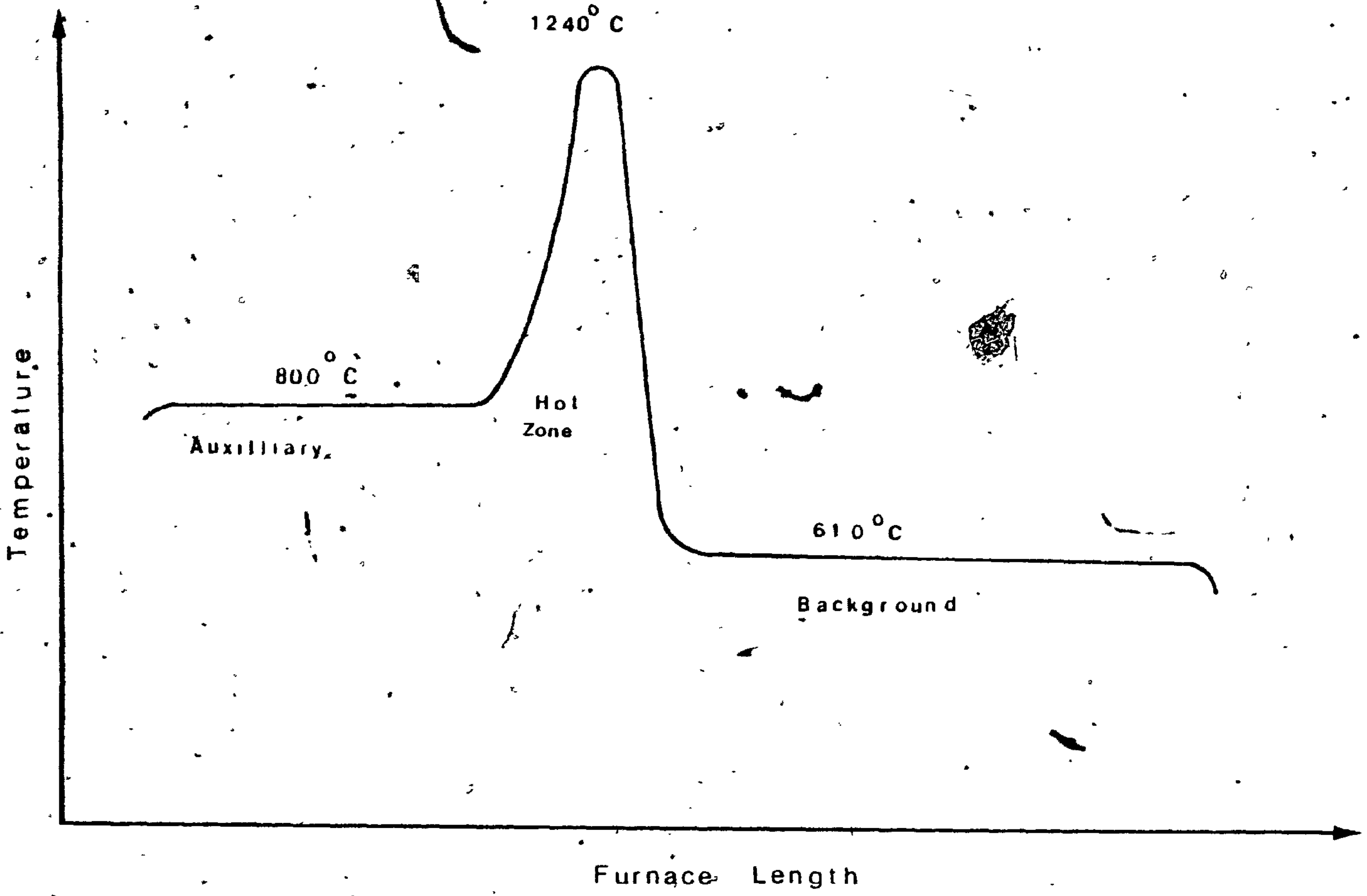

Fig. 3-1 DESIRED TEMPERATURE OF ZONE MELTING FURNACE

zone towards the auxilliary furnace, the auxilliary furnace can be used for annealing.

If the gradient between the hot zone and the auxilliary furnace is not sufficiently steep, it is advisable to have growth towards the background furnace. This eliminates the need for precise control of the auxilliary furnace. Satisfactory results can be achieved by connecting it in parallel with the hot zone through appropriate transformers.

3.2 Heating arrangement

In all systems where high temperatures are involved (above 1200°C), heating elements exposed to atmospheric conditions undergo severe oxidation corrosion. Hence, very few choices of heaters exist. In zone melting (specially GaAs), high temperatures have to be maintained in a narrow zone in a relatively open system. This severely limits the space for the heating element and makes requirements more demanding.

Induction heating, though convenient, is not very suitable for crystal growth unless used with a heat susceptor. In addition, induction heating is difficult to control. Optimum frequency is a function of the resistivity of the material to be melted. As the resistivity of GaAs ranges from 10^{-4} to 10^{+8} Ω-cm, the efficiency of the system would be questionable.

Resistive heating is the most common and best controllable method. In an oxidizing atmosphere, the highest temperatures can be

obtained from heating elements of the platinum-rhodium alloys. Unfortunately, the resistivities of platinum base alloys are so low that in order to achieve a reasonable working resistance (.5 - 1Ω), very thin wire must be used. This necessitates the imbedding of the wire in high temperature ceramics such as very high purity (min. 99%) alumina (Al_2O_3). As alumina is a good thermal insulator, for a given furnace temperature, the temperature of the imbedded element is substantially higher (approximately 200 - 300°C) than an exposed element.

Though platinum is a noble metal and does not seem to oxidize, in fact, the oxide is not stable and sublimes; hence, there is a gradual loss of metal, specially at elevated temperatures. In view of the above considerations, the first furnace design was as shown in Figure 3.2 The hot zone heating elements were silicon carbide, the background and auxiliary temperatures were achieved with the use of heat pipes.

3.3 Principle and Characteristics of Heat Pipes (3.2)

For this application, a heat pipe consists of a closed double jacket tube internally lined, with a wick usually made from the same alloy as the double jacket tube. The wick is saturated with a working fluid and evacuated of all non-condensable gases.

Heat supplied by an external heat source causes evaporation of the working fluid in the high temperature region of the heat pipe (evaporator). Due to the pressure differential between hot and cold regions, the vapour is transported towards the colder region of the

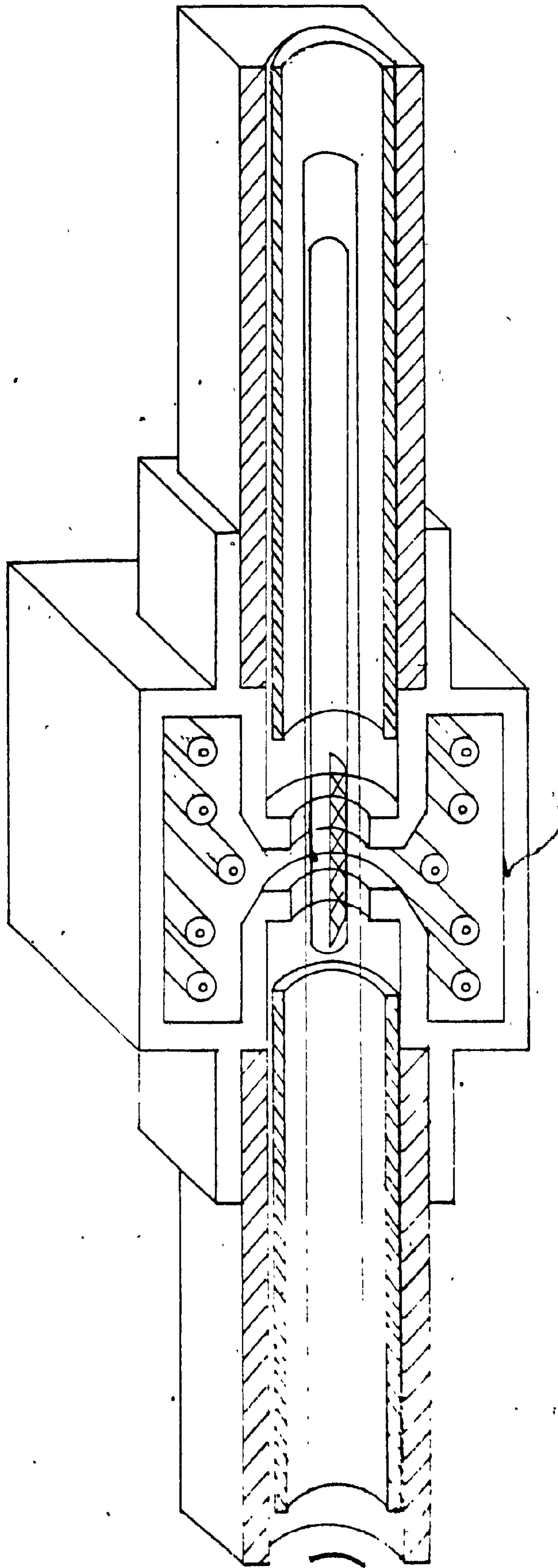

Fig. 3.2 INITIAL FURNACE DESIGN

pipe and condenses (condesor region), releasing the latent heat of evaporation. The condensed liquid is then recycled to the high temperature evaporator region by capillary action of the wick, in some cases assisted by gravity.

The axial rate of heat transfer in a heat pipe is essentially equal to the latent heat flux in the evaporator (3.2)

$$Q = \dot{m}_v L \qquad [3.1]$$

where Q = heat transfer rate (cal/sec)

$\dot{m}_v$ = vapour mass flow rate at evaporator exit (gr/sec)

L = latent heat of vaporization of the liquid (cal/gr)

For a tubular pipe equation [3.1] becomes:

$$Q = A_v \rho \bar{V} L \qquad [3.2]$$

where A_v = vapour passage cross-sectional area (cm^2)

ρ = vapour density (gr/cm^3)

$\bar{V}$ = average vapour velocity (cm/sec)

The high conductivity of the heat pipe creates an adiabatic region situated between the condensor and evaporator regions, where, for example, in the case of a sodium heat pipe operating at 900°C, the temperature gradient is approximately 0.01°C/cm, and the heat transfer is approximately 2500 Watts (3.2). The length of the adiabatic section depends on the specific configuration, (that is along how much of the length of the heat pipe, heat is applied), and can vary between one third to three quarters of the overall length of the heat pipe.

The working fluid should have the following properties:

a) It should be any element or non-dissociable compound (e.g., Freon, Ammonia) which in the operating range of the heat pipe, will be in liquid form and have a vapour pressure of at least 1 KPa proper heat transfer. For safety reasons the vapour pressure should not be much higher than 1000 KPa.

b) It should be compatible with the wall material and the wick, i.e., it should wet but should not react with them.

c) The working fluid should have a large latent heat of vaporization, and preferably a low viscosity.

The mesh size of the wick material depends on the viscosity of the liquid working fluid.

The maximum heat transfer rate is limited by the maximum flow rate of the condensed liquid through the wick (3.3). For tubular pipes the flow rate can be expressed by

$$Q = \sigma A_w DL/b\nu\ell \qquad [3.3]$$

where σ = the surface tension of the liquid working fluid (dynes/cm)

A_w = the free flow area of the wick (cm^2)

D = wick pore size (cm)

ν = the kinematic viscosity of the liquid working fluid (cm^2/sec)

b = capillary geometric constant (dimensionless, of the order of 20 for wire mesh capillary)

ℓ = length of the heat pipe (cm)

The thermal conductivities of the heat pipes are several orders of magnitude higher than the best metallic conductors. The major limitation of present heat pipes is the high temperature oxidation corrosion and the reduction in strength of the wall material at elevated temperatures. The most common high temperature alloys commercially available (in pipe form) are the stainless steels.

The temperature limitations of stainless steel are specified by their scaling temperatures. This is the temperature at which the oxide layers are no longer adherent and flake off (hence scaling temperature). Above this temperature, the oxidation rate is not parabolic but linear (much higher). Therefore, for safety reasons, heat pipes should not be used above the scaling temperature of the wall material. Table 3.1 lists some of the physical properties of the most common types of stainless steels. However, it should be noted that not all shapes such as plate, pipe, bar, etc., are available in each type of stainless steels.

During this investigation many heat pipes of different sizes, using each of the following working fluids: Na, K, Cs, Cd and Li, were tested. Table 3.2 lists some of the physical properties and Figure 3.3 shows the theoretical power capability of some working fluids. For the operating temperature of 610°C, the best results were obtained with sodium, in agreement with published data (3.5).

The advantages of the heat pipe for crystal growth are two-fold; firstly, it provides a constant temperature necessary for the background furnace without the need of the complicated multizone furnaces, and secondly, it provides a sharp gradient necessary for a zone melting furance. The dimensions of heat pipes shown in Figure 3.2 were as follows: a 600 mm long heat pipe provided the background temperature with an isothermal length of approximately 200 mm. The heat pipe in the auxilliary furnace had a length of 375 mm and was designed to anneal the grown crystal. The respective temperatures of the heat pipes were achieved by varying their positions with respect to the hot zone. Only the hot zone temperature was monitored and controlled. The furnace was made to travel while the ampule was held stationary in order to avoid vibration. Travel was achieved through the use of a D.C. Variable speed motor and appropriate gear reducers. The growth rates were varied from 6 to 20 mm/hr.

3.4 Heat Pipe Construction

The most readily available stainless steel pipes are type 304, therefore this type was initially chosen. A "three inch" pipe with outside diameter (O.D) of 88.9 mm and inside diameter (I.D.) of 72.5 mm and a "four inch" pipe with O.D. of 114.3 mm and I.D. of 101.7 mm nominal sizes were chosen from standard pipe sizes. An arbitrary length of 600 mm was chosen for the first heat pipe. Two end plates resembling large washers were machined to fit in between the two pipes (also of stainless steel type 304). A fill tube with 9.5 mm O.D. and 3.2 mm I.D. was also machined. The extra heavy wall

			304	304L	309	309S	310	310S	316	316L	321	347
Heat Resistance:	Maximum Operating Temperature - Intermittent Service	°F	1600	1600	1850	1850	1900	1900	1600	1600	1550	1550
		°C	871	871	1008	1008	1036	1036	871	871	842	842
	Continuous Service	°F	1700	1700	1950	1950	2050	2050	1700	1700	1650	1650
		°C	926	926	1063	1063	1120	1120	926	926	898	898
Thermal Expansion	Expansion- (In./In./°Fx10^{-6})	32°-212°F	9.6	9.6	8.3	8.3	8.0	8.0	8.9	8.9	9.3	9.3
		0°-100°C	17.3	17.3	14.9	14.9	14.4	14.4	16.0	16.0	16.7	16.7
	(cm/cm/°Cx10^{-6})	32°-1200°F	10.4	10.4	10.0	10.0	9.7	9.7	10.1	10.1	10.7	10.7
		0°-650°C	18.7	18.7	18.0	18.0	17.5	17.5	18.2	18.2	19.3	19.1
Thermal Conductivity:	Conductivity (B.T.U./ft.^{2}/hr/°F/ft)	at 212°F	9.4	9.4	8.0	8.0	8.0	8.0	9.4	9.4	9.3	9.3
		at 100°C	16.3	16.3	13.8	13.8	13.8	13.8	16.3	16.3	16.1	16.1
	(J/m^2/S/°C/m)	at 932°F	12.4	12.4	10.8	10.8	10.8	10.8	12.4	12.4	12.8	12.8
		at 500°C	21.5	21.5	18.7	18.7	18.7	18.7	21.5	21.5	22.2	22.2

Table 3.1 Physical and Mechanical Properties - 300 Stainless Steels (3.4).

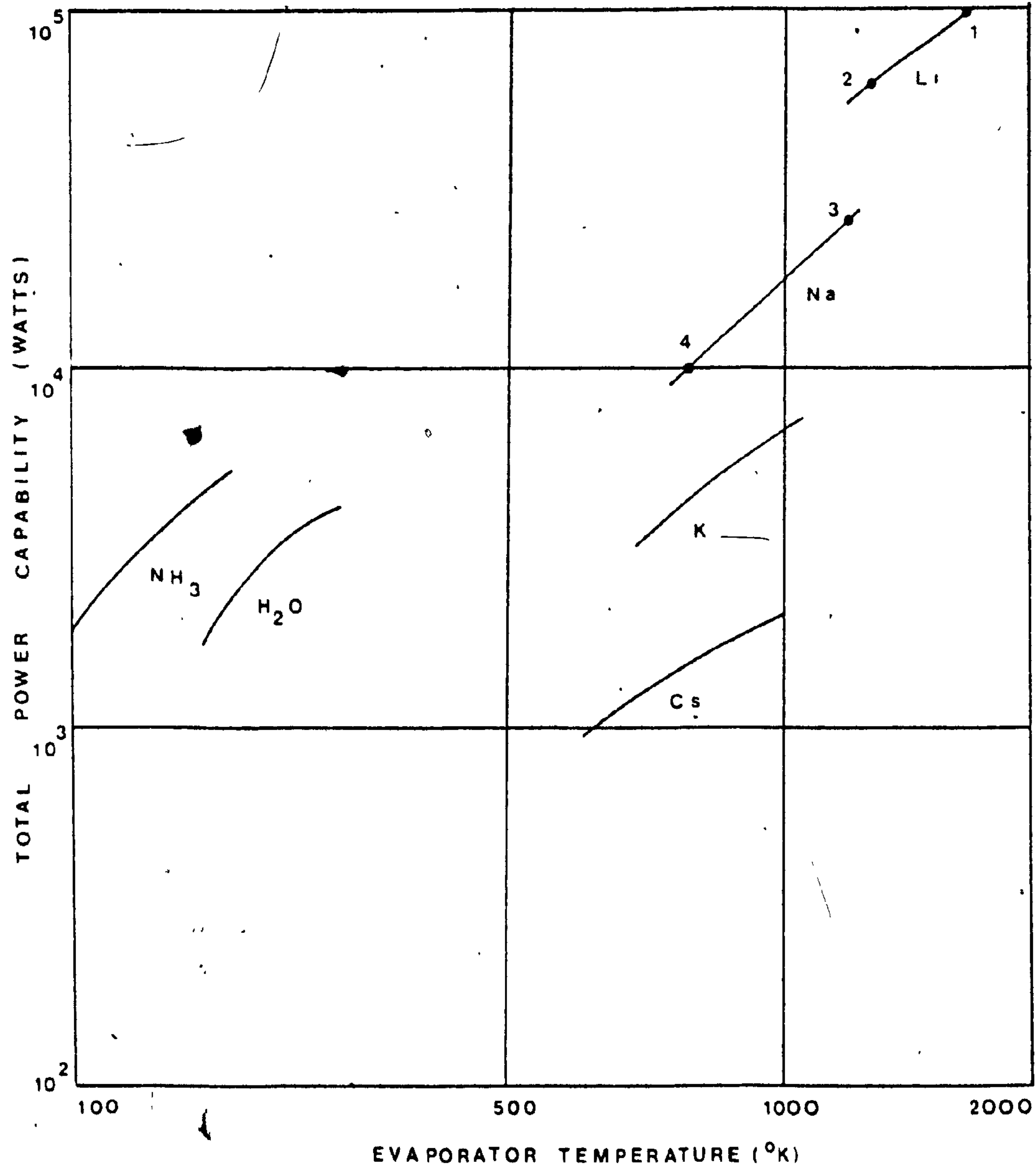

Fig. 3.3 Theoretical working fluid heat transfer capability

Table 3.2 Selected Working Fluid Characteristics (3.3)

Working Fluid	Melting Point °C	Boiling Point °C	Density at M.P. gr/cm^3	Latent Heat* cal/gr	Surface Tension at M.P. gr/cm
Ammonia	-77	-333	.68*	327.5	2.8×10^{-3}
Water	0	100	.998	540	11.7×10^{-3}
Cesium	29	705	1.79	146	8.2×10^{-3}
Potassium	64	760	.82	496.5	15.8×10^{-3}
Sodium	98	883	.93	1006	28.4×10^{-3}
Lithium	179	1317	.51	4693	59.4×10^{-3}
Lead	327	1737	10.48	205	67.1×10^{-3}
Indium	156	209	6.98	469	94×10^{-3}
Silver	960	2212	9.28	556	138.8×10^{-3}

* At one atm. pressure

was specially chosen to prevent buckling during the subsequent crimping process.

A hole was drilled into one of the end plates to fit in the fill tube. The plain end plate was welded to one end of the pipes. Two stainless steel screens, one 325 mesh, and the other 150 mesh, were loosely wrapped together (3 layers each) and placed in between the pipes. The second end plate with the fill tube facing outward was welded to the open end of the pipes.

The inside of the structure was degreased and etched with HF: HNO_3: H_2O (3:10:87) solution and dried. It was then helium leak tested for possible cracks or pin holes in the weld regions.

A special stainless steel funnel with vacuum seals and viewing window was built. The nozzle was thin enough to fit the fill tube. The funnel was connected to the structure; input and output ports enabled the evacuation and pressurization of the system.

The system was evacuated and then filled with inert gas (argon). The solid working fluid was transferred to the funnel, the system was sealed and then heated to the melting point of the working fluid. Upon pressurization of the funnel, the molten working fluid was forced into the structure. The funnel was removed, the structure evacuated and the fill tube crimped and welded. The resulting heat pipe was thoroughly tested.

This procedure was successfully implemented for all the heat

pipes regardless of size or type of wall material. A schematic diagram of a heat pipe is shown in Figure 3.4.

3.5 Heating Element Considerations

Silicon carbide heating elements were chosen for the hot zone for their high temperature service limit, ease of availability, and low cost. The elements had a nominal 10 mm diameter, 200 mm heating length, and 600 mm overall length. The heaters were available in one shape only (like a rod, solid or spiral) with different contact arrangements (both contacts on same or opposite sides). Originally, two were positioned above the ampule and two below it, perpendicular to the axis of the ampule as shown in Figure 3.2. The resulting axial temperature profile is shown in Figure 3.5. It can be seen that the hot zone was very narrow and the gradients very steep. The flat zone in the background heat pipe was approximately 200 mm long, hence this was the maximum length of crystals that could be grown. The ampule was placed in a SiC support tube to prevent sagging. The ends of the support tube were attached to vibration free posts independent of the furnace. The radial clearance between the furnace bore and the support tube was about 10 mm radial.

The first furnace had a short life due to the insufficient power capacity of the four elements and, the severe oxidation corrosion of the stainless steel (type 304) heat pipes. Because the hot zone thermocouple was bare, the temperature was not very stable with fluctuations of ± 20°C.

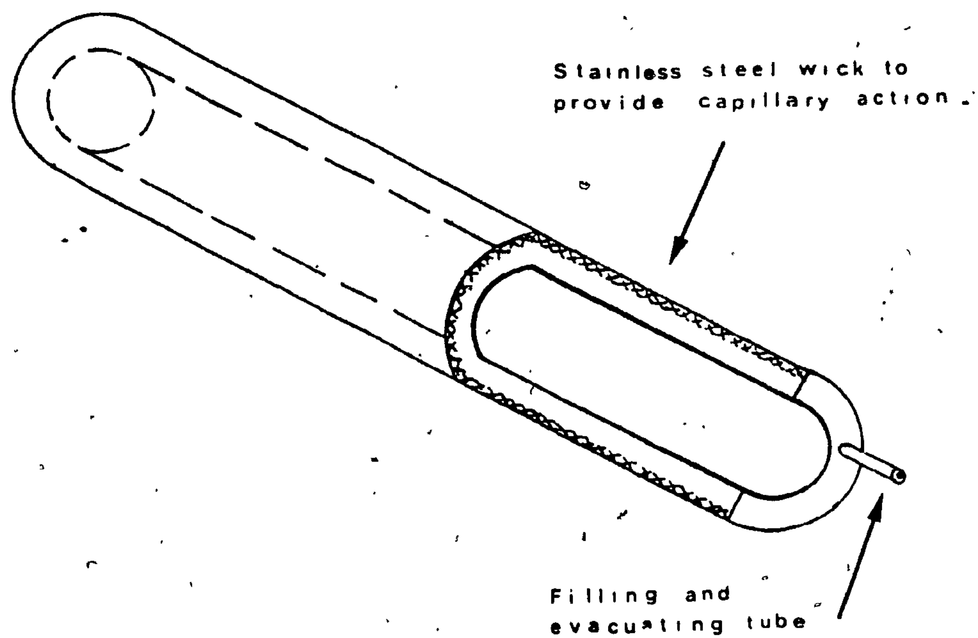

FIG. 3.4 CROSS-SECTIONAL VIEW OF HEAT PIPE

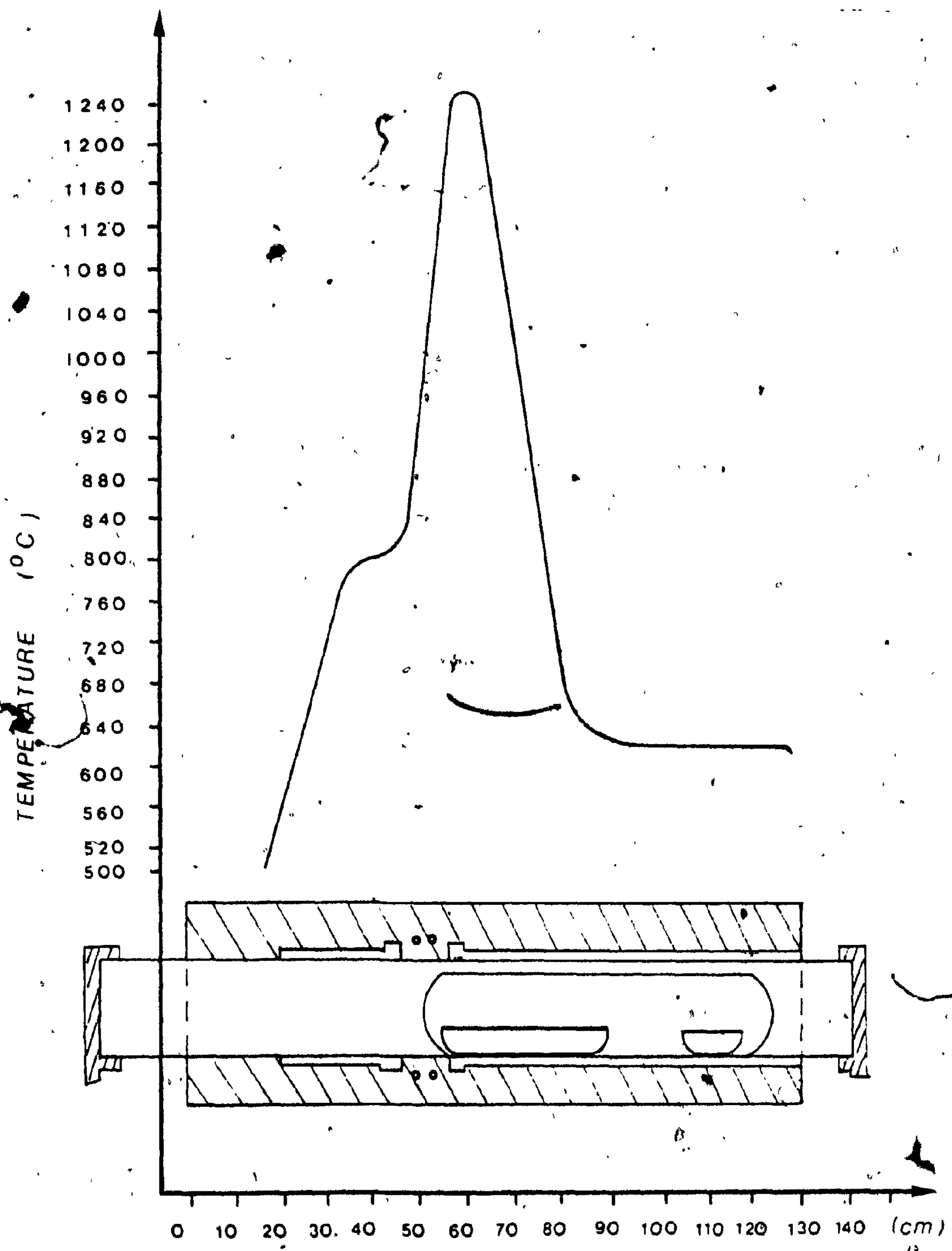

Fig. 3.5 FURNACE TEMPERATURE PROFILE

The power capacity of the furnace was increased by installing larger diameter heating elements (19 mm diameter) as well as increasing the number of elements from 4 to 10. The heat pipe wall material was changed from stainless steel type 304 (scaling temperature 925°C) to type 310 (scaling temperature 1150°C). The length of the background furnace was increased to 900 mm and alumina caps were used to protect the evaporator ends of the heat pipes, as well as to decrease the orifice size of the furnace.

The life expectancy was greatly improved, but the temperature profile deteriorated. The adiabatic region of the longer (900 mm) background heat pipe was even shorter than the previous furnace, and as the furnace travelled (ampule stationary) the temperature in the heat pipes changed.

Preliminary results indicated that the silicon carbide heaters, specially, used in this configuration (Figure 3.2) were not suitable for large cross-section crystal growth. An undesirable property of these heating elements is their change of resistance with time and temperature (in a non-linear manner). This change is more than 100%. Furthermore, the large manufacturing tolerances in resistivities made it impossible to find matched sets; hence, results were not reproducible. Most important of all, as the heaters were supplied only in straight rods, the resulting furnace configuration did not provide a uniform radial temperature distribution; and finally, their fragility did not allow any mechanical stresses. This made tight fittings impossible,

resulting in large convection currents that disturbed the temperature control.

To better understand the solidification process, a view port was deemed necessary. This was easily accomplished with the SiC furnace, since the heaters did not totally surround the ampule. Nucleation, interface shape, and rate of solidication were studied in depth. It was found that initially the freezing rate did not correspond to the rate of displacement of the furnace. The crystal remained molten for a considerable length of time, followed by a fast freezing rate, and finally, solidification continued at the rate of furnace travel. This indicated super-cooling, where the temperature of the melt dropped below the melting point of the crystal, until the excess energy was large enough to induce nucleation. With the first nucleation, the solidifying liquid rejected heat to the melt, thereby raising the temperature of the melt to the melting point of the compound. Thereafter, steady state was achieved. It was also observed that initially the solid liquid interface was highly concave with respect to the solid, and within a length of 20 mm, the shape of the interface changed to slightly convex. Furthermore, the interface was not symmetric, and its shape did not remain constant.

It was evident at this point that in order to achieve reproducible results, a new hot zone heater with much better radial temperature distribution was necessary.

3.6 New heating element and furnace design:

Of all the metallic alloys, only two choices existed, namely the Platinum alloys (previously discussed) and KANTHAL Al (iron base alloy). After careful consideration KANTHAL Al was chosen.

The maximum recommended element temperature of Kanthal Al alloy is 1375°C. Since this was very close to the melting point of GaAs (1238°C), it was evident that the element should be exposed in order to freely radiate it's heat. For a conservative design, the power density at 1375°C, as suggested by the manufacturer was 9.3 KW/m^2 of area. From previous experience with the globar elements, the hot zone power consumption was approximately 6 KW, therefore the heating element required a radiating surface area of 0.645 square metres.

Kanthal alloy was available in two shapes, round wire and rectangular strip. The first attempt was to make a heating element as shown in Figure 3.6. This element had a capacity of 11 KW, the resulting interface was very symmetric, indicating uniform radial temperature distribution, and as the element was totally surrounded with insulation, convection currents were minimized. The hot zone power requirements decreased to 3 KW, and its control was facilitated.

The heat pipes for the auxilliary and background temperature zones were heated by separate heaters. A steep gradient was achieved by a water cooled jacket placed between the hot zone and the background furnace.

Fig. 3.6 KANTHAL A1 Strip Heater

Though the shape of the solidifying interface was slightly convex as desired, no single crystals were grown with this configuration because of the supercooling problem. The hot zone element did not last as long as expected because the proximity of the windings to each other hindered adequate radiation. The temperature of the heater rose excessively and the strips buckled.

The results of the Kanthal strip heater indicated that with proper design and insulation a heater having a capacity of 3KW was sufficient. This made possible the use of round wire, the latter being more self supporting than the strip. The thickest commercially available was 8.25 mm in diameter. Calculating the surface area of the wire, a design consisting of three concentric coils was adopted. The spacing between the windings of all the coils was 2.54 mm (.1 inch), while the spacing between proximal coils was 6.35 mm (.25 inches). The power capacity of the heater based on a power density of .94 KW/m^2 was 4.9 KW. As the round wire heater had better radiating capability than the rectangular strip heater, for the same furnace temperature (1240°C), the element temperature dropped to 1300°C and the power consumption decreased to 2KW.

It should be emphasized that the minimization of power requirements is significant not only from a cost point of view, but it also makes possible the use of Kanthal Al alloy. This eliminated the need of silicon carbide or Platinum heating elements.

During the course of this study, it was decided to investigate the growth of GaAs crystals with larger cross-section; hence larger silicon carbide support tubes were necessary. Previous observations had shown that with zone melting, since a narrow zone is held at high temperatures only, the ampule did not sag. In effect, the SiC support tube was not necessary. This facilitated observation of the crystal and eliminated the heat losser due to conductivity of the SiC tube.

3.7 Final Design; Dynamic Temperature Profile:

As mentioned earlier, the initial furnace design had several shortcomings. The heat pipe temperatures were not controlled. The length of the crystals was limited by the length of the flat zone in the background furnace; and, the heat pipes had a limited lifetime due to the oxidation corrosion of the wall material. To eliminate these undesirable features, the design was modified as follows (Figure 3.7): the two stationary heat pipes were eliminated and the sharp gradient, required for the solidifying interface, was achieved through the use of a water-cooled jacket. The auxilliary and background temperature zones each had a separate heater, the auxilliary heater was connected in parallel with the hot zone, with the thermocouple placed in the hot zone. The background furnace heater consisted of a three zone heater and was connected to a separate controller. A small heat pipe was attached to a stainless steel extension pipe; and, this in turn was attached to a vibration free post outside the furnace.

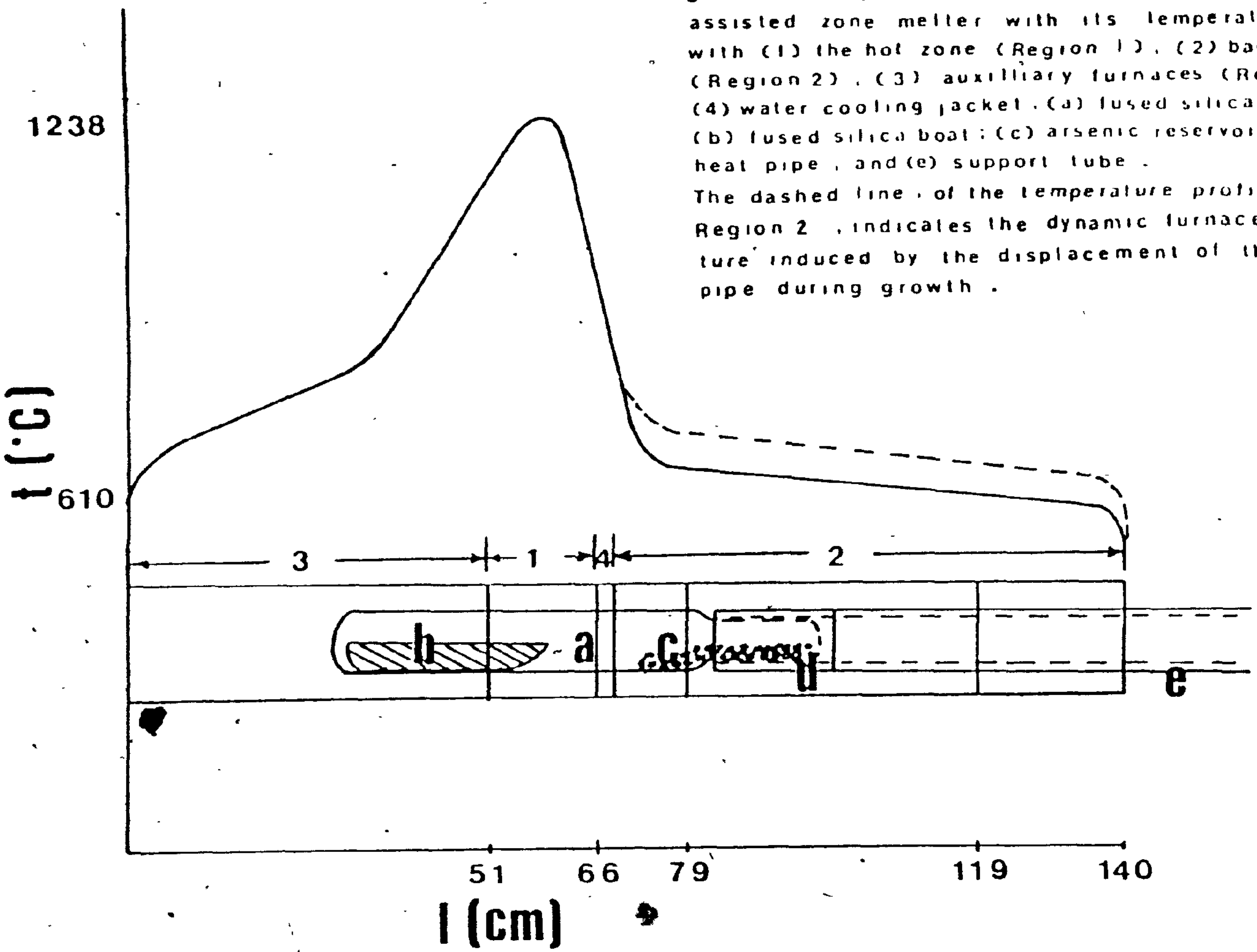

Fig. 3.7 Final furnace temperature profile. Schematic representation of the heat pipe assisted zone melter with its temperature profile with (1) the hot zone (Region 1), (2) background (Region 2), (3) auxilliary furnaces (Region 3); (4) water cooling jacket. (a) fused silica ampule; (b) fused silica boat; (c) arsenic reservoir; (d) heat pipe, and (e) support tube.
The dashed line, of the temperature profile of Region 2, indicates the dynamic furnace temperature induced by the displacement of the heat pipe during growth.

The thermocouple of the background furnace controller was inserted into the small heat pipe (between the walls). The end of the ampule was inserted into the heat pipe and both the heat pipe and ampule remained stationary, while the furnace travelled. The position of the background control thermocouple facilitated the temperature measurement and control. In effect, the final design accomplished a truly three zone furnace where the background control was heat pipe assisted.

The heat pipe was never exposed to very high temperatures (613°C, well below scaling termperature); hence, it had practically an unlimited life, and the length of the crystal was not limited by the length of the flat zone.

The electrical circuit diagram is shown in Figure 3.8. Temperature controllers C1 and C2 were of high precision type with proportional, derivative, and integral control. (Barber-Colman model 543). Power units P1 and P2 were phase angle control (stepless) type. The hot zone thermocouple was type R (Pt - Pt 13 Rh) while for the background it was type K (chromel-alumel). Zone 2 of the furnace consisted of three heaters. The power was adjusted through auto-transformers T3 and T5 to produce a relatively constant temperature.

Similarly in Zones 1 and 3, by adjusting auto-transformer T1, the power in Zone 3 was adjusted to produce the approximate desired temperature. Since the thermocouple for controller C1 was placed in Zone 1, the temperature in Zone 3 was not precisely controlled but it

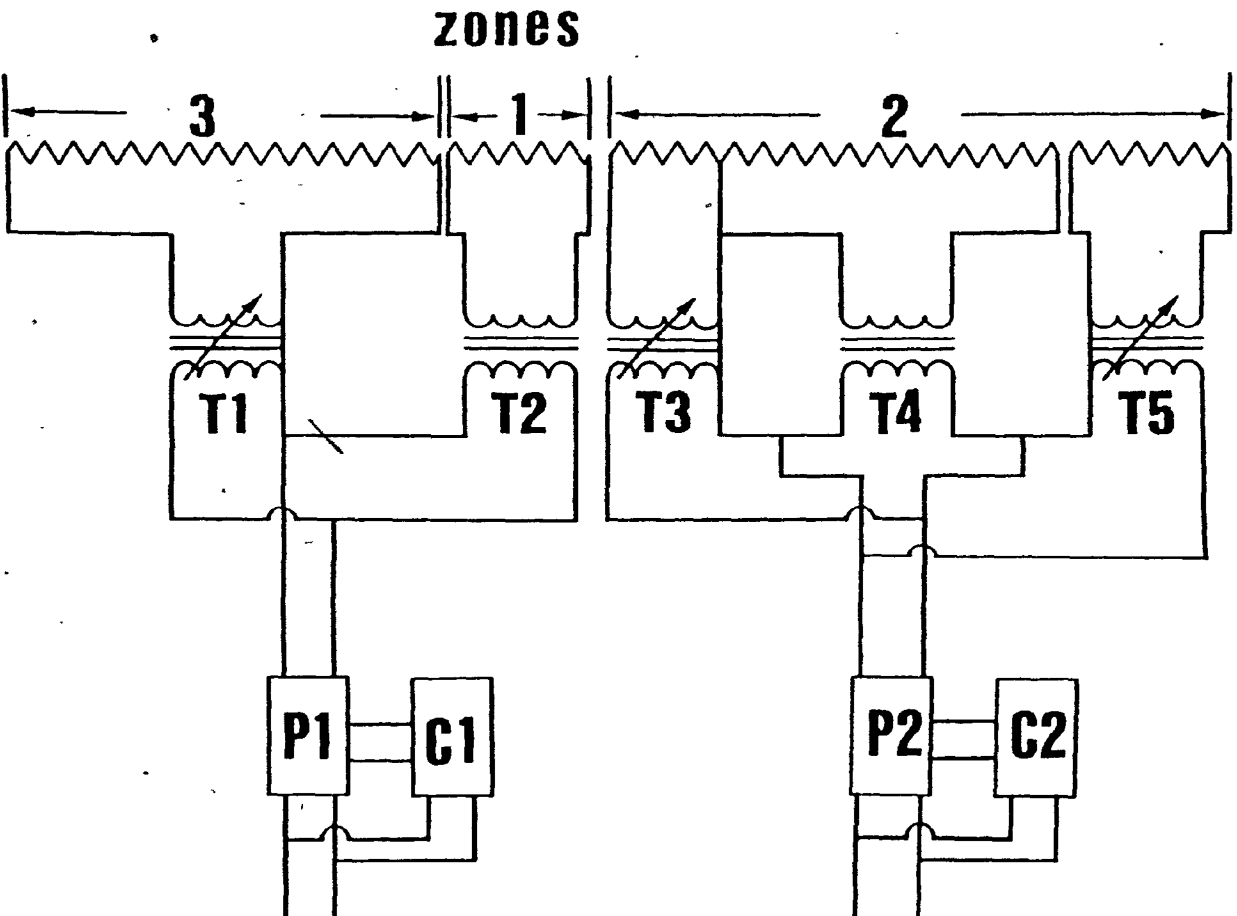

Fig. 3-8 Circuit diagram furnace control system. P_1 and P_2 are phase angle control power supplies (10 kW). C_1 and C_2 are precision controllers with 4 to 20 mA output signal. T_1, T_3 and T_5 are variable auto transformers; while T_2 and T_4 are step-down transformers.

was always kept higher than the temperature in Zone 2.

This system gave reproducible results as well as long life. The only remaining problem was the initial sudden nucleation which resulted in a polycrystalline tip. In turn, this polycrystalline tip acted as a seed and the grains propagated. It is to be noted that if a seed crystal is used, an inherently stable configuration is achieved, supercooling does not exist, and as the seed is single the ingot also grows as a single crystal.

3.8 Nucleation Control

In the case of single crystal growth, control of nucleation without affecting the purity of the melt is very difficult. It is common practice to make the tip of the boat pointed. This minimizes the cross-sectional area and reduces the number of possible spurious nucleations.

Usually boats are made by taking a round tube of a given length (approximately 20 cm) sealing the ends (one end pointed and the other rounded) and cutting it lengthwise. The cross-sectional area is semi-circular and usually the outside diameter is approximately equal to the inside diameter of the ampule, hence when the boat is placed in the ampule there is a large surface contact between the boat and the ampule.

As the tip of the boat is pointed (similar to a cone split in half), it is not in contact with the ampule (see Figure 3.7). Heat losses at the tip occur through radiation and convection; while in the

main body of the crystal, conduction also contributes to heat loss. This change in heat losses due to change in dimension of cross-section affects the shape of the solid liquid interface and increases supercooling.

Several boat designs were tested but none were found to be satisfactory. Large rounded tips increased the chances of multinucleations, while pointed tips resulted in more pronounced supercooling. It was evident that the pointed tip was desirable, if a means of heat transfer from the tip of the crystal could be devised.

The final solution was the design of a double tip boat as shown in Figure 3.9. The front compartment was filled with chunks of GaAs and upon melting, it formed a perfect contact with the wall of the inside tip. The first and second tips were approximately 50 mm apart; therefore, when the second tip was in the hot zone, the first tip was 50 mm away. It had solidified and was in a significantly lower temperature region (approximately 70°C lower). The large mass of the first tip acted as a good heat sink for the second tip.

Because all commercially grown crystals are seeded for properly oriented growth, the initial nucleation problem does not exist. However, the above mentioned technique is a good means of growing seed crystals of any size as well as growing large crystals without seeding.

Several crystals were grown with different resistivities (3.6). Semi-insulating samples with chrome doping had resistivities as high as $5 \times 10^{8}\Omega$-cm, while undoped samples had resistivities of $10^{-2}\Omega$-cm.

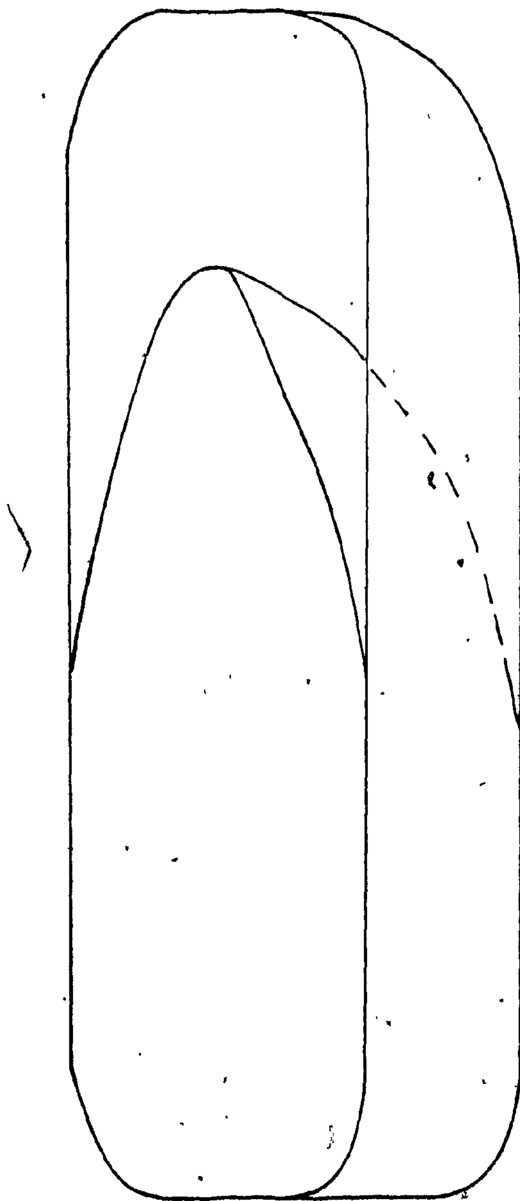

Fig. 3.9 Double tip boat.

All crystals had very shiny bottoms, indicating that the reaction with the boat was minimal. The edges were well rounded, indicating non-wetting. Due to the zone melting technique, there were no distortions in the boat walls, thus the grown crystals had uniform cross-section within the tolerances of the fused silica tubes. The last 25 mm (last molten zone length) turned polycrystalline irrespective of the length. The maximum length of the boat that could be accommodated was 300 mm, and therefore, the maximum length of a single crystal that could be grown was 275 mm.

3.9 Ampule preparation:

The boats were sand blasted with 50 μm alumina powder followed by ultrasonic rinses in trichloroethylene, acetone and water. It was then soaked for 10 minutes in HNO_3: HCL (1:1) solution for passivation of the surface, and finally rinsed thoroughly (several times) with distilled water (3.7).

The ampule was also degreased in trichloroethylene and acetone followed by a 15 minute etch in 10% HF solution, and finally rinsed several times with distilled water. All the components were dried under an infra-red lamp.

Stoichiometric amount of 6N gallium was placed in the boat and stoichiometric amount of arsenic plus an excess amount (required to maintain the vapour pressure in the ampule) were placed in the ampule. The ampule was connected to a vacuum pump, evacuated of all gases (10^{-5} torr), and sealed.

All three zones of the furnace were simultaneously raised to 618°C, following which the hot zone and auxilliary zone were raised to their respective temperatures. After a stabilization period of 30 to 60 minutes, growth was initiated.

The primary insulation used was Resco RS17A castable Alumina with service temperature of 1800°C and the secondary insulation (backing) was Fiberfax Alumina fibre insulating felt with service temperature of 1250°C.

The furnace travelled on Thomson linear bearings and motion was achieved with a lead screw coupled to a D.C. variable speed motor with a 9000:1 speed reducer.

CHAPTER 4

CHARACTERIZATION

The crystal growth experiments showed that it is possible to synthesize and grow single crystals in a single step. This minimized the contamination and decreased the cost. Figure 4.1 shows a picture of a crystal grown in this furnace and table 4.1 lists the impurities detected by Spark source mass spectrographic analyses listed in chronological order (4.1). It can be seen that the impurity concentrations are at least as low as the best LEC grown crystals, and the number of impurities are few, (4.2, 4.3). Figure 4.2 shows typical dislocation densities. Different etchants were tried, for the SI samples the A/B etch was used consisting of a solution of 2 ml H_2O, 8 mg $AgNO_3$, 1 g CrO_3 and 1 ml of HF (4.4). For the low resistivity samples the AHA etch was used consisting of NH_4OH in distilled H_2O with a pH range of 10.6 to 13.4 and current densities between 0.1 and 2 mA/cm^2 (etching times were between 1 and 5 minutes), (4.5).

Several factors affect the dislocation density. Two of the most important are the arsenic vapour pressure during growth (4.6), and the gradient at the freezing interface. This study was not extended to optimize these parameters. As it is very difficult to measure the absolute temperature, the best method would be to grow a series of crystals and find the particular temperature (this might vary depending on actual set up) which yields the minimum dislocation density, and similarly vary the temperature gradient thereby varying the shape of the solid liquid interface. This is a rather lengthy procedure and is beyond the scope of this study.

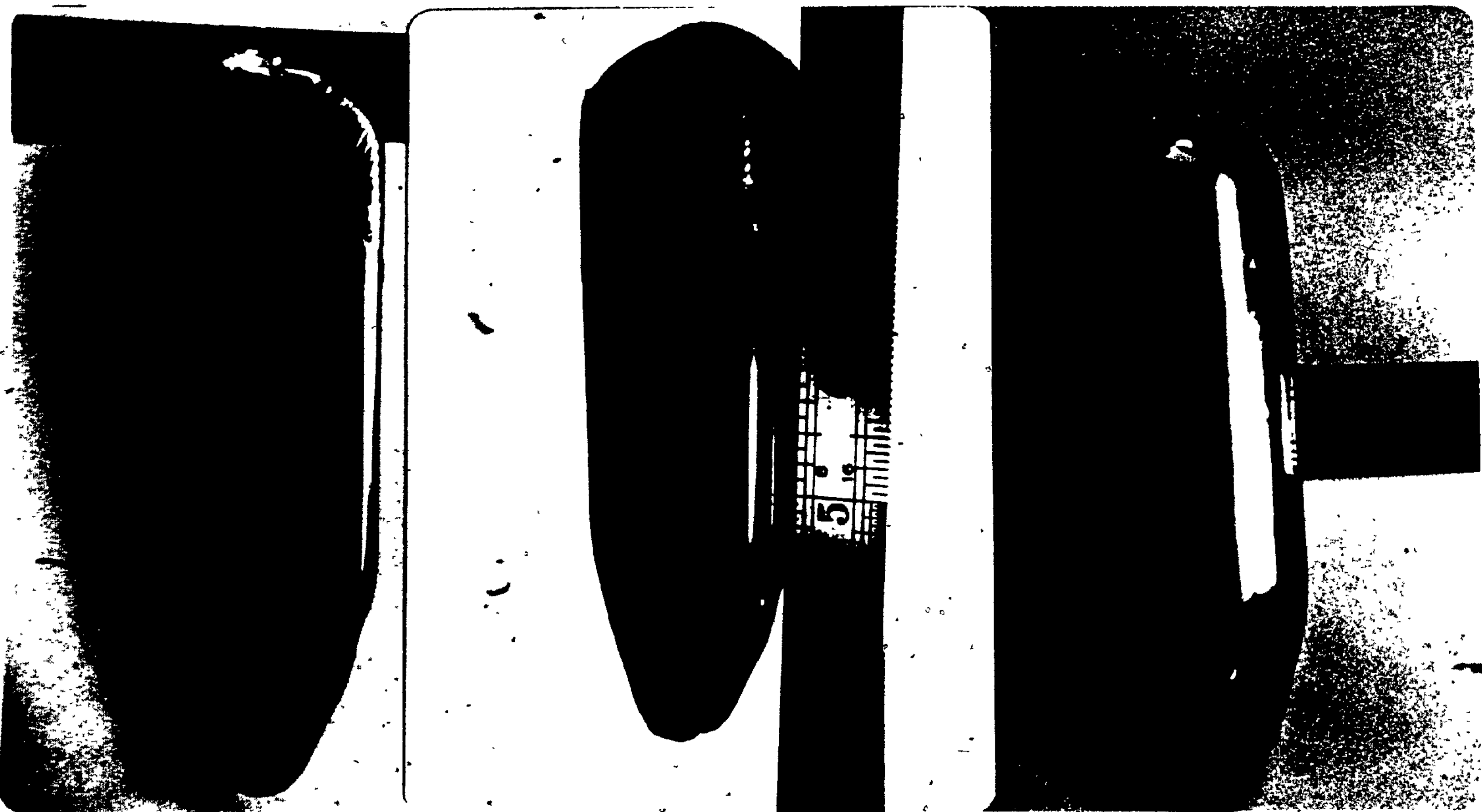

Fig. 4.1 Top and Bottom view of a crystal grown by Zone Melting

SAMPLE	1		2		3		4		5	
CHARACTER	SC		SI		SC		SI		SC	
BOAT MATERIAL	FUSED SILICA		FUSED SILICA		BORON NITRIDE		FUSED SILICA		FUSED SILICA	
impurity	ppm atomic	at.cm^{-3} x10^6	ppm atomic	at.cm^{-3} x10^{16}	ppm atomic	at.cm^{-3} x 10^{16}	ppm atomic	at.cm^{-3} x10^{16}	ppm atomic	at.cm^{-3} x 10^{16}
C	1.0	4.0	0.3	1.3	0.4	1.8	0.6	2.6	0.6	2.6
N_2	0.3	1.0			0.3	1.3	0.1	0.4	0.02	0.09
O_2	4.0	17.0	0.2	0.9	0.4	1.8	0.4	1.8	1.0	4.0
Na	Intf.*	Intf.	Intf.	Intf.	Intf.	Intf.	Intf.	Intf.	Intf.	Intf.
Mg	0.01	0.4								
Al	0.1	0.4	0.1	0.4	0.2	0.9	0.02	0.09	0.2	0.9
Si	1.0	4.4	0.1	0.44	1.0	4.4	0.2	0.9	0.2	0.9
S	0.08	0.4	0.06	0.3	0.06	0.3	0.1	0.4	0.04	0.18
K	0.01	0.04	0.05	0.2	0.03	0.1	0.03	0.1	0.01	0.04
Ca			0.005	0.02			0.005	0.02	0.003	0.01
Cr	0.3	1.3	0.7	3.1			1.0	4.4		
Fe	0.03	0.1								
Sb						0.03	0.1			

Table 4.1 Spark source mass spectrographic analyses of gallium arsenide samples 1 to 5, for trace impurites, the concentrations are semiquantitative.

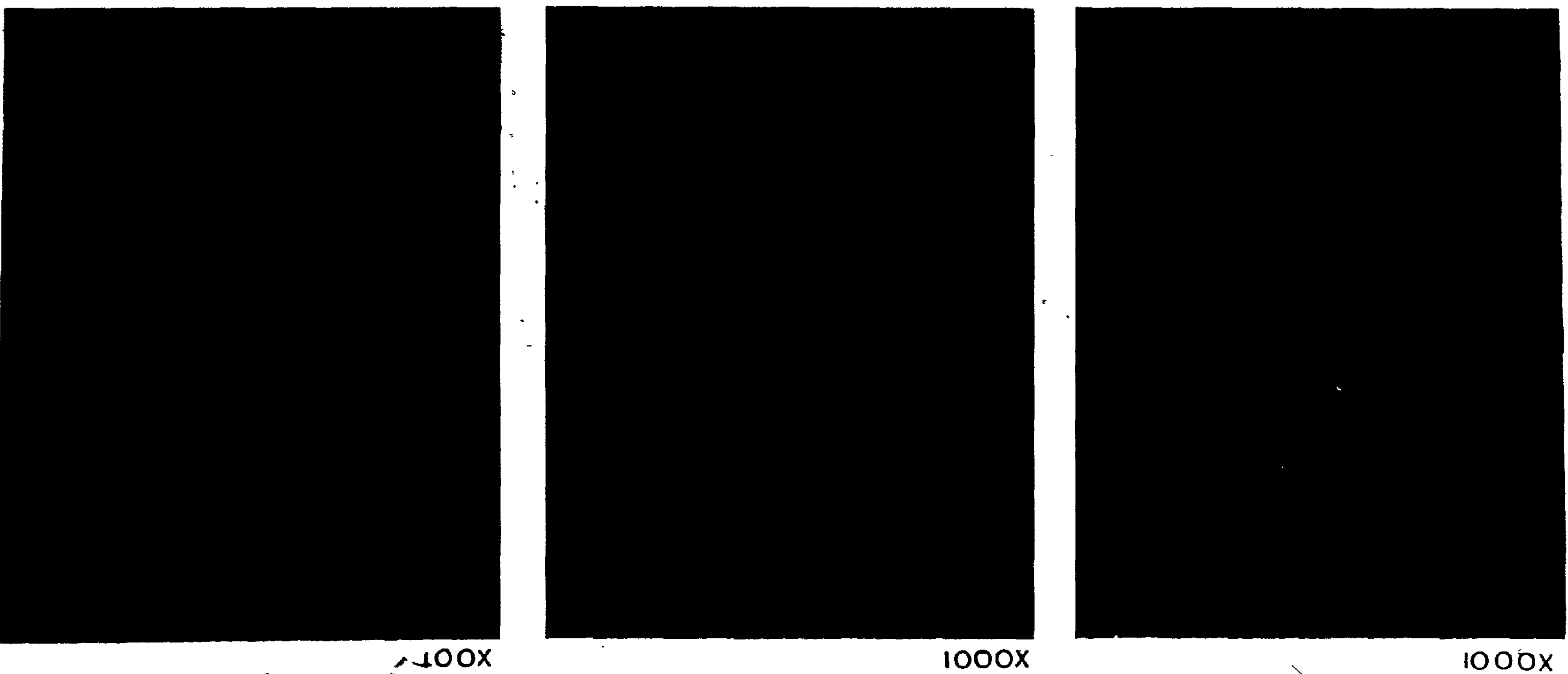

Fig. 4.2 Typical Dislocations in GaAs

The first attempt to measure transport properties was to measure photocurrent. Excitation with a monochromator at room temperature did not indicate any change in the photocurrent corresponding to any deep levels. Two light sources were used: a quartz lamp, and a Xenon lamp. As the power output of the monochromator as a function of wavelength did not remain constant, the photocurrent was proportional to the power of the incident light.

Hall effect apparatus was set up to measure the transport properties. A stainless steel tube of 0.25 mm wall thickness was used to suspend the sample into the Dewar. The crystals were cut into slices with a wire saw, then lapped to 1 mm thickness. Brass masks were machined and Hall samples were prepared by jet cutting with alumina powder. Figure 4.3 shows the configuration of the samples. The dimensions were according to A.S.T.M. standards (4.7), and the double leg configuration was chosen to compare measurements on both pairs as well as to have a spare set in case of accidental loss. Ohmic contacts were achieved by using a gold germanium alloy (88% Au, 12% Ge by weight, and 5.5 mg of Ni added) (4.8); the constituents were placed in a tungsten crucible and evaporated at 10^{-6} Torr pressure. Germanium, gold and nickel evaporated consecutively. The samples were then placed in a tube and heated to 450°C in a reducing atmosphere. This temperature was maintained for 3 minutes. The germanium diffused into the GaAs and created an n^+ region. The Ni prevented the gold from balling. The contacts were checked and wires soldered with indium solder.

The samples were mounted on a copper block with Teflon insulation. The temperature was controlled with an ordinary controller using a platinum resistance sensor. Stability was within 0.1°C. Low noise shielded cable with appropriate feed throughs (type Brüel and Kjaer) were employed for the conductors. A Keithley model 225 nano-amp current source was used for power source. The sample voltage was measured with a Keithley model 616 digital electrometer. In the case of semi-insulating samples, the sample resistance was of the order of 10^{10} ohms, therefore, an electrometer was necessary and the voltage was measured at the power supply terminals, as the lead wire resistance was insignificant with respect to the sample resistance. Current values were kept to a minimum (less than 1nA), to insure that the I^2R value was negligible and the only heat source was the copper block. In the case of semiconducting samples, the voltage across the sample was measured across and independent set of wires connected to the sample and not across the power supply as the wire resistance was found to be significant. The two configurations are as shown in Figure 4.4.

In the case of semiconducting samples, the Hall voltages were measured with a Hewlett Packard model 3455 A digital Multimeter, but for the semi-insulating samples the input impedance of the multimeter ($10^7\Omega$) was not satisfactory. A Keithley model 602 analog electrometer (battery operated) with a unity gain output was used as a low noise high input impedance isolation stage. All the measurements and calculations were performed according to ASTM specifications. Hall voltage measurements were taken for all possible configurations (by reversing the magnetic field and the direction of the current, and repeated for

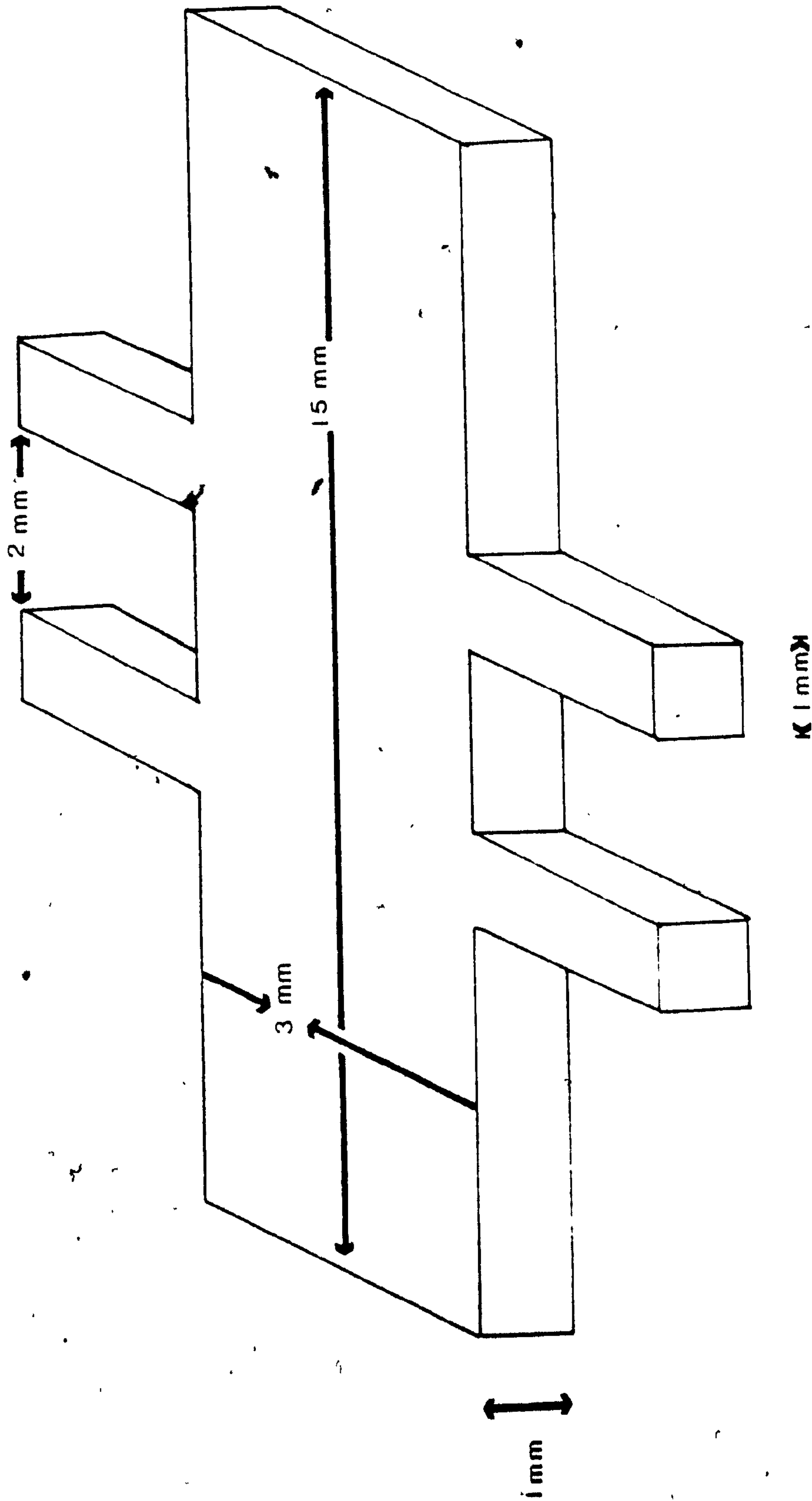

Fig. 4.3 Hall sample dimensions.

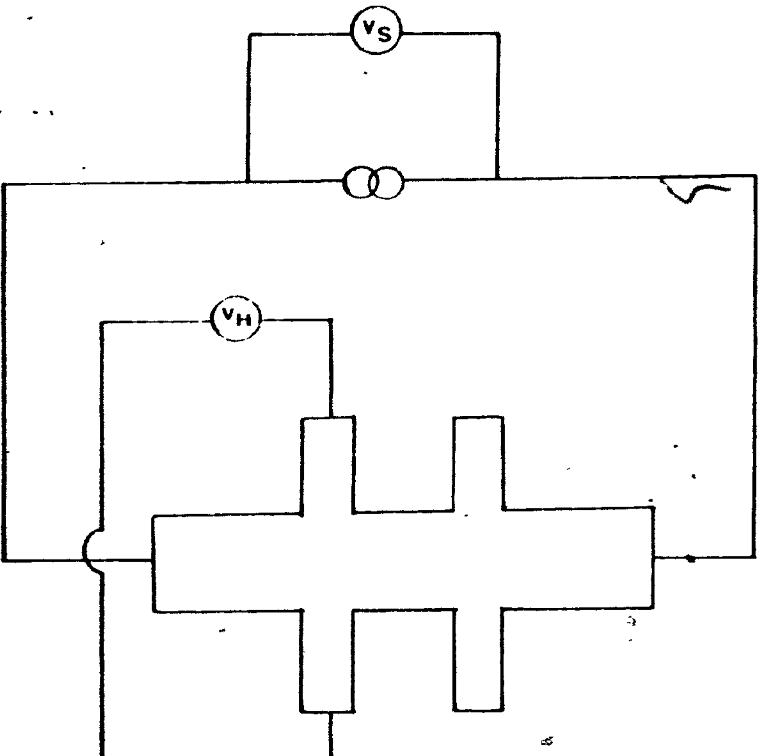

SEMI-INSULATING ARRANGEMENT

SEMICONDUCTING SAMPLES

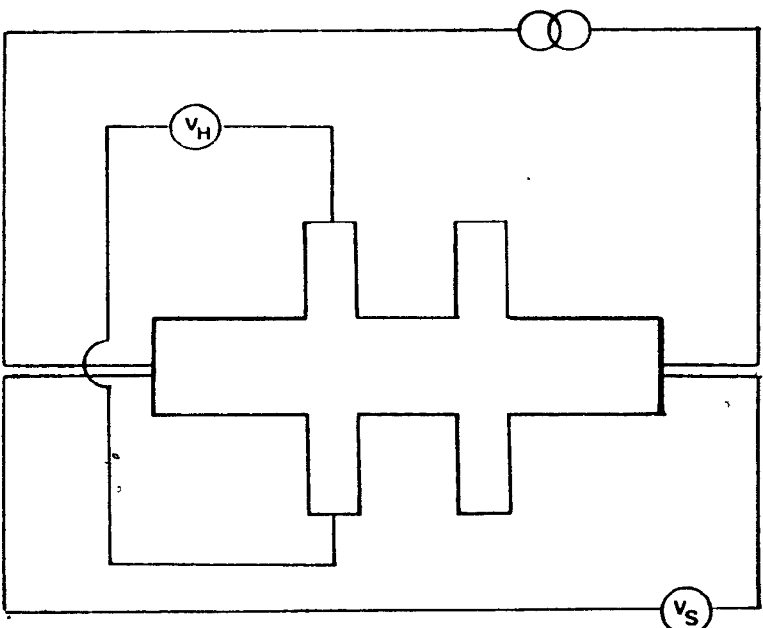

V_S - Sample Voltage
V_H - Hall Voltage

Fig. 4.4 Measurement arrangement.

increasing and decreasing temperatures). The data was averaged to eliminate errors due to misalignment of the legs, according to A.S.T.M. standards.

4.1 Analyses:

Many articles have appeared (2.13 - 2.18) analyzing and proposing models for deep lying impurities. The models have progressively become more accurate as more and more impurities have been taken into account. Starting with one deep impurity (chrome doping), followed by two deep impurities (oxygen and chrome), and extended to 2 deep and 2 shallow impurities.

Since electrical measurements do not reveal the chemical nature of the impurities, it is customary to perform chemical analyses and relate the electrical measurements to the chemical analyses. The two accepted methods of chemical analyses are spark source mass spectrographic analyses (MSA) and secondary ion mass spectroscopy (SIMS). The detection limit of the MSA is 1 ppb and the measurements are termed semiquantitative, i.e. the accuracies are within a factor of three. Electrical measurements being much more sensitive, the concentrations indicated by MSA are adjusted, to conform to the electrical measurements. This is achieved by increasing the concentrations of some impurities and decreasing others, but in all cases the adjustments are well within the uncertainty of the MSA results.

Usually 10-20 impurities are indicated by MSA with concentrations ranging from 1 ppb to 10^2 ppm. Of these, two deep lying and 2 shallow lying impurities with the highest concentration are chosen

(typically Si shallow donor, C shallow acceptor, O deep acceptor trap and Cr deep donor trap) and the remainder neglected. Since in effect adjusting the concentration of every impurity corresponds to 1 degree of freedom, adjusting four impurity concentrations corresponds to 4 degrees of freedom; hence, many solutions satisfying the charge neutrality conditions can be found with a slight variation in the Fermi level.

As our samples had relatively few impurities, a multilevel model (4.9) was employed to consider the effect of all the impurities determined by MSA. The position of the Fermi level was calculated based on the charge neutrality condition and correlated to the measured transport properties.

The charge neturality condition is given as follows*:

$$n + \sum_{i=1}^{\ell} N_{ai}^{-} = p + \sum_{j=1}^{m} N_{dj}^{+} \qquad [4.1]$$

where N_{ai}^{-} and N_{dj}^{+} are the ionized acceptor and donor concentrations respectively. It is assumed that the Fermi level is within the forbidden energy region, i.e. several kT units away from the band edges, especially in the SI GaAs. Therefore Maxwellian statistics can be used. The the intrinsic electron n, and hole p concentrations are given by the well known expressions:

$$n = N_c \exp. \left(- \frac{E_g - E_f}{kT}\right) \qquad [4.2]$$

and

$$p = N_v \exp. \left(- \frac{E_f}{kT}\right) \qquad [4.3]$$

The energy gap E_g, taken from the top of the valence band with its

*See Appendix A.

temperature dependence of Eg can be given by the Varshni equation (4.10):

$$E_g(T) = 1.522 - \frac{5.8 \times 10^{-4} T^2}{(T + 300)} \qquad [4.4]$$

$N_c = 2(2\pi m_e^* kT/h^2)^{3/2}$ is the effective density of state in the conduction band

$N_v = 2(2\pi m_h^* kT/h^2)^{3/2}$ is the effective density of state in the valence band

The effective density of state masses of electrons m_e and holes m_h are given by (4.11)

$$m_e^* = .068\ m_o \qquad m_h^* = .538\ m_o$$

Calculated from $m_h^* = (m_{lh}^{3/2} + m_{hh}^{3/2})^{2/3}$

$$= (0.12^{3/2} + 0.50^{3/2})^{2/3}$$

where m_{lh} and m_{hh}, are the masses of the light and heavy holes. m_o being the rest mass of the electron.

$k = 1.380 \times 10^{-23}$ joule/° K is the Boltzmann's constant

$h = 6.625 \times 10^{-34}$ joule-sec is Planck's constant.

The different impurity concentrations can be determined by the two terms summed over the different acceptors $i = 1$ to ℓ, and donors $j = 1$ to m, knowing the specific doping concentrations N_{ai}, N_{dj} and the ionization energies, E_{ai}, E_{dj} of the species, respectively.

The ionized acceptors' concentration is given by:

$$N_{ai}^{-} = N_{ai}(1 + 1/g \exp \frac{E_{ai} - E_f}{kT})^{-1} \quad [4.5]$$

and the expression for the ionized donors' concentration is:

$$N_{dj}^{+} = N_{dj}(1 + g \exp \frac{E_{dj} + E_f - E_g}{kT})^{-1} \quad [4.6]$$

The degeneracy factor, g, was taken to be 4 for shallow acceptors, and 2 in the case of donors. For deep lying acceptors the degeneracy factor was also taken as 2, since the influence of the double degenerate valence band on the deep lying acceptor levels can be neglected.

Equation [4.1] , taking into account all the intrinsic and extrinsic charge carriers with the expressions [4.2] to [4.6], could be solved algebraically to determine the Fermi energy, but becomes very tedious for calculating multilevel cases. Therefore, instead of introducing simplified assumptions (4.12, 4.13, 4.14), the numerical computer solution of the system of equations [4.1] to [4.6] was performed in this investigation. Figures 4.5 to 4.9 show graphically n, p, N_{ai}^{-} and N_{dj}^{+} as a function of energy (4.15). The ionized donors and acceptors correspond to all the impurities indicated by MSA.

The energy levels of the electrically active impurities detected in our crystals were taken as follows: Carbon shallow acceptor with E_{ai} = 0.019eV, oxygen deep lying donor with E_{d1} = 0.68eV, silicon shallow donor with E_{d2} = 0.002eV, sulphur shallow donor with E_{d3} = 0.006eV, Chromium deep lying acceptor with E_{a2} = 0.9eV.

The ionization energies for the shallow impurities were taken from Sze's work (4.16), while the values for the deep lying levels were obtained from Lin's data (2.13, 4.17). It is to be mentioned that although the assignment of the deep lying donor level to oxygen was argued in the literature (4.18), its entity is generally accepted. However, from the point of view of this analysis, only the existence of a deep donor level is of importance.

The sign of the Hall coefficient indicates whether the crystal is n or p type. The Hall coefficient is given as follows:

$$\varepsilon_H = R_H JB \qquad [4.7]$$

where

ε_H = Hall field

R_H = Hall coefficient

J = current density

B = magnetic field strength

if the sample is of length L, width w, and thickness t, then the Hall voltage:

$$V_H = \varepsilon_H w \qquad [4.8]$$

the current through the sample:

$$I = Jwt \qquad [4.9]$$

Therefore,

$$\varepsilon_H = \frac{V_H}{w} = \frac{R_H IB}{wt} \qquad [4.10]$$

hence,

$$R_H = \frac{tv_H}{IB} \qquad [4.11]$$

t, V_H, I and B being known or measured, therefore R_H can be calculated.

The sample resistance:

$$R = \frac{V_s}{I} \qquad [4.12]$$

where V_s is the voltage across the sample, also;

$$R = \rho \frac{L}{wt} \qquad [4.13]$$

where ρ is the resistivity from [4.12] and [4.13]

$$\rho = \frac{V_s wt}{IL} \qquad [4.14]$$

In the presence of donors and acceptors:

$$J = e(nu_n + pu_p)\varepsilon \qquad [4.15]$$

where n and p are the number of donors and acceptors per unit volume, u_n and u_p, are the respective mobilities, e is electronic charge and ε is the electric field in the direction of current flow, then the hall coefficient R_H is given by (4.19)

$$R_H = \frac{R_1\sigma_1^2 + R_2\sigma_2^2}{(\sigma_1 + \sigma_2)^2}(r) \qquad [4.16]$$

where

$R_1 = -\frac{1}{ne}$, $R_2 = \frac{1}{pe}$ and r is the scattering factor

conductivities are $\sigma_n = enu_n$, $\sigma_p = epu_p$

hence,

$$\text{resistivity } \rho = \frac{1}{\sigma_1} + \frac{1}{\sigma_2} = (enu_n)^{-1} + (epu_p)^{-1} \qquad [4.17]$$

and the scattering factor

$$r = \langle \tau^2 \rangle / \langle \tau \rangle^2 \qquad [4.18]$$

where τ is the mean free time between carrier collisions.

It has been reported (4.20) that for GaAs above 100°K, phonon scattering dominates over ionized impurity scattering, and it has been shown (4.21) that for phonon scattering $r = \frac{3\pi}{8} = 1.18$, while for ionized impurity scattering $r = \frac{315}{512} = 1.93$. Equation [4 .11] allows the calculation of the experimental Hall coefficient, while equation [4.16] yields the theoretical one.

4.2 Results and Discussion:

Using the above described multilevel model to determine the position of the Fermi level, (Figure 4.5 - 4.9), all the significant electrically active impurities and the resulting charge carriers were taken into account. The calculated results show that samples 1,3 and 5 are n-type semiconductors with the Fermi levels at 1.39, 1.39 and 1.35 eV respectively; 2 and 4 are semi-insulators with the Fermi levels close to the centre of the gap at 0.71 and 0.72 eV. The results are summarized in Table 4.2.

The experimental results indicated that the amount of impurities introducing negative charge carriers were systematically under-rated in the mass-spectrographic data.

SAMPLE	1	2	3	4	5
Ef(eV)	1.38	0.65	1.39	0.63	1.3
$R_H(cm^3C^{-1})$ (Ca)	$-9.7x10^1$	$4.5x10^{10}$	$-6.6x10^1$	$2.3x10^{10}$	$-2.1x10^3$
$R_H(cm^3C^{-1})$ (Me)	$-2.0x10^1$	$1.0x10^{12}$	-	-	$-1.1x10^2$
$n(cm^{-3}$ (Ca)	$6.4x10^{16}$	$3.5x10^4$	$9.5x10^{16}$	$1.6x10^4$	$2.9x10^{15}$
$n(cm^{-3})$ (Me)	$3.1x10^{17}$	$6.2x10^6$	-	-	$5.7x10^{16}$
$p(cm^{-3})$ (Ca)	0.0	$1.2x10^8$	-	$2.6x10^8$	-
$\mu_H(cm^{-2}v^{-1}sec^{-1})$ (Me)	3600	2267	-	-	4728
ρ(ohm cm) (Ca)	$1.1x10^{-2}$	$1.3x10^8$	$7.7x10^{-3}$	$6.0x10^7$	$2.5x10^{-1}$
ρ(ohm cm) (Me)	$5.8x10^{-3}$	$4.4x10^8$	$1x10^{-4}$	-	$2.4x10^{-2}$

Table 4.2. The measured (Me) and calculated (Ca) Hall coefficients (R_H), electron (n), hole (p) concentrations, mobilities (μ_H), and resistivities (ρ) of samples 1 to 5.

In all other investigations, the concentrations of the impurities indicated by MSA have been readjusted (within the margin of uncertainty of the MSA) to compensate for the differences between electrical and chemical results. In our investigation since the only shallow donor was silicon its concentration had to be increased to represent the measured donor concentration. It is to be noted that our crystal growth experiments indicated that an excess pressure of arsenic together with the sandblasting of the crucible eliminated wetting. The excess arsenic pressure was not considered detrimental as there was no published data relating it to the electrical properties. Hence, all the crystals were grown arsenic rich.

It is evident that in compound semiconductors, in addition to Schottky and Frenkel defects, two more possible defects can occur. First, an antisite defect where in a compound crystal, AB, an atom of element A may occupy an anion (B-type) lattice site B_A. Second, an antistructure pair $B_A A_B$, this could result from interchanging two nearest neighbouring atoms in the perfect zinc-blende or wurtzite structure.

Based on thermodynamic consideration it has been calculated, (4.22), that in GaAs the density of antistructure defects at 1100°K is $2 \times 10^{19}/cm^3$ and 2×10^{15} at 500°K. The experimentally (EPR) measured value was found to be $5 \times 10^{19}/cm^3$. However, because they are neutral within unit cell they should not be prominent in the luminescence or absorption spectra and will not affect the carrier concentration (4.22).

In the case of antisite defects in GaAs, theoretical calculations indicate (4.22) that their density should be less than the density of antistructure defects.

It has been reported (4.23) that a phase extent exists in GaAs. The variation of Arsenic extends from 49.998% to 50.009% with corresponding lattice constants of 5.65326 A° to 5.65298 A° respectively at 20°C. In effect the lattice constant decreases with increased arsenic content. This would only be possible if the excess arsenic atoms occupy substitutional position in the lattice (the arsenic atom being smaller than the gallium atom) in which case they are electrically active. Calculating the number of possible excess donors arising from the phase extent,

$$\text{number of unit cells per cm}^3 = \left[\frac{1}{5.65298 \times 10^{-8}}\right]^3$$

$$= 5.53564 \times 10^{21}$$

number of arsenic atoms per unit cell = 4

hence, number of atoms per cm^3 = 22.14255×10^{21} atoms/cm^3

taking 0.009% (the excess As atom) = 1.9928×10^{18} atoms/cm^3

which is in agreement with theoretical calculations.

Taking into consideration two electrons per excess arsenic atom the phase extent corresponds to 4×10^{18} donors per cm^3. Since Arsenic is one of the constituents of GaAs, it is not considered an

impurity. This could account for the mass spectrographically undetected donor concentration. If the phase extent is accounted for, the MSA levels would not have needed any readjustment. Recently, the 0.82 eV (EL2) deep level has been associated with the antisite defect (4.24) further supporting the existence of electrically active antisite defects.

Subsequent to this investigation, using a Bridgman type apparatus it has been shown that the dislocation density is a function of the arsenic vapour pressure (4.6). Furthermore, in another investigation, our assumption has been verified where using an LEC type apparatus, it has been shown that (4.25) the electrical properties including donor and acceptor concentrations as well as mobility are drastically affected by the phase extent.

The results of our investigation led us to the following conclusion. Assuming that all the electrically active impurities are either donors or acceptors, their position in the energy gap of the material is characterized by their respective ionization potentials. Then, if the sum of the shallow ionized donor concentrations is N_D, the sum of the shallow ionized acceptor concentrations is N_A, the deep lying donor and acceptor concentrations are N_{Dd} and N_{Ad} respectively, the following four cases can be distinguished.

The material is n-type if:

1) $(N_D - N_A) > 0$ [4.19]

it is semi-insulating if:

1a) $(N_D - N_A) < N_{Ad}$ [4.20]

it is semiconducting if:

$$(N_D - N_A) > N_{Ad} \quad [4.21]$$

In this case, the concentration of the deep lying donor has negligible influence.

The material is p-type if:

$$(N_D - N_A) < 0 \quad [4.22]$$

it is semi-insulating if:

$$2a)\ (N_A - N_D) < N_{Dd} \quad [4.23]$$

it is semiconducting if:

$$2b)\ (N_A - N_D) > N_{Dd} \quad [4.24]$$

In this case, the concentration of the deep lying acceptor has negligible influence.

These conditions are in complete agreement with the calculated data and the experimental values collected in Tables 4.1 and 4.2.

The theoretical and experimental resistivities and Hall coefficients were also calculated using equations [4.11] to [4.17]. The electron and hole mobilities were taken from known curves (4.26) as a function of ionized impurity concentrations. The results are fairly acceptable and are listed in Table 4.2.

The results of Hall effect measurements of three Cr-doped semi-

insulating GaAs crystals are reported in Table 4.3. The measured resistivities, ρ, and Hall coefficients, R_H, are used to calculate by the previously given, well-known expressions, the electron concentration n, the Hall mobility, μ_H, as well as the $\ln(R_H e T^{3/2})^{-1}$ expressions. The latter is used to construct the Arhenius plot to deduce the position of the Fermi level based on the measured data as it is shown in Figure 4.10.

Equation [4.20] gives the requirement to achieve SI GaAs by chrome doping. It is to be noted that this equation is not valid for concentrations for Cr beyond the solid solubility limit. Thus it cannot be taken for granted that the addition of Cr will necessarily compensate any amount of shallow donors.

It is of interest to notice that sample 2 of Table 4.3 is the same as the one of Table 4.1 and 4.2. The good agreement of the position of the Fermi level (E_f = 0.71 eV) calculated by the multi-level model and the one determined from the measured transport properties (E_f = 0[illegible]4 eV) is quite remarkable (see Table 4.3 and Figure 4.10). This underlines the suitability of the multilevel model as a powerful tool for analysis of transport properties. Also, it can indicate the existence of the phase extent and its effect on the transport properties.

	T(K)	ρ(ohm cm)	$R_H(cm^3C^{-1})$	$n(cm^{-3})$	$u_H(cm^2v^{-1}s^{-1})$	(E_g-E_f)eV	E_f(eV)
Sample 2	303	$4.4x10^8$	$1x10^{12}$	$6.2x10^6$	2270	0.789	0.64
	349	$7.42x10^6$	$2.07x10^{10}$	$3x10^8$	2790		
	379	$8.13x10^5$	$2.29x10^9$	$2.73x10^9$	2817		
	424	$5.5x10^4$	$1.1x10^8$	$5.7x10^{10}$	2000		
Sample 7	290	$2.7x10^8$	$4.83x10^{11}$	$1.29x10^7$	1790	0.602	0.827
	300	$1.16x10^8$	$2.64x10^{11}$	$2.36x10^7$	2280		
	347	$5.54x10^6$	$1.92x10^{10}$	$3.25x10^8$	3470		
	372	$4.72x10^5$	$1.63x10^9$	$3.84x10^9$	3680		
Sample 8	298	$3.58x10^8$	$6.92x10^{11}$	$9.02x10^6$	1930	0.628	0.802
	322	$5.13x10^7$	$1.38x10^{11}$	$4.52x10^7$	2700		
	347	$7.46x10^6$	$2.16x10^{10}$	$2.88x10^8$	2900		
	372	$1.26x10^6$	$3.75x10^9$	$1.66x10^9$	2980		

Table 4.3 Results of Hall effect measurements of Cr doped semi-insulating GaAs, samples 2, 7, and 8. The positions of the Fermi levels are determined from curves of Figure 4.10 according to [4.1].

Fig. 4 5

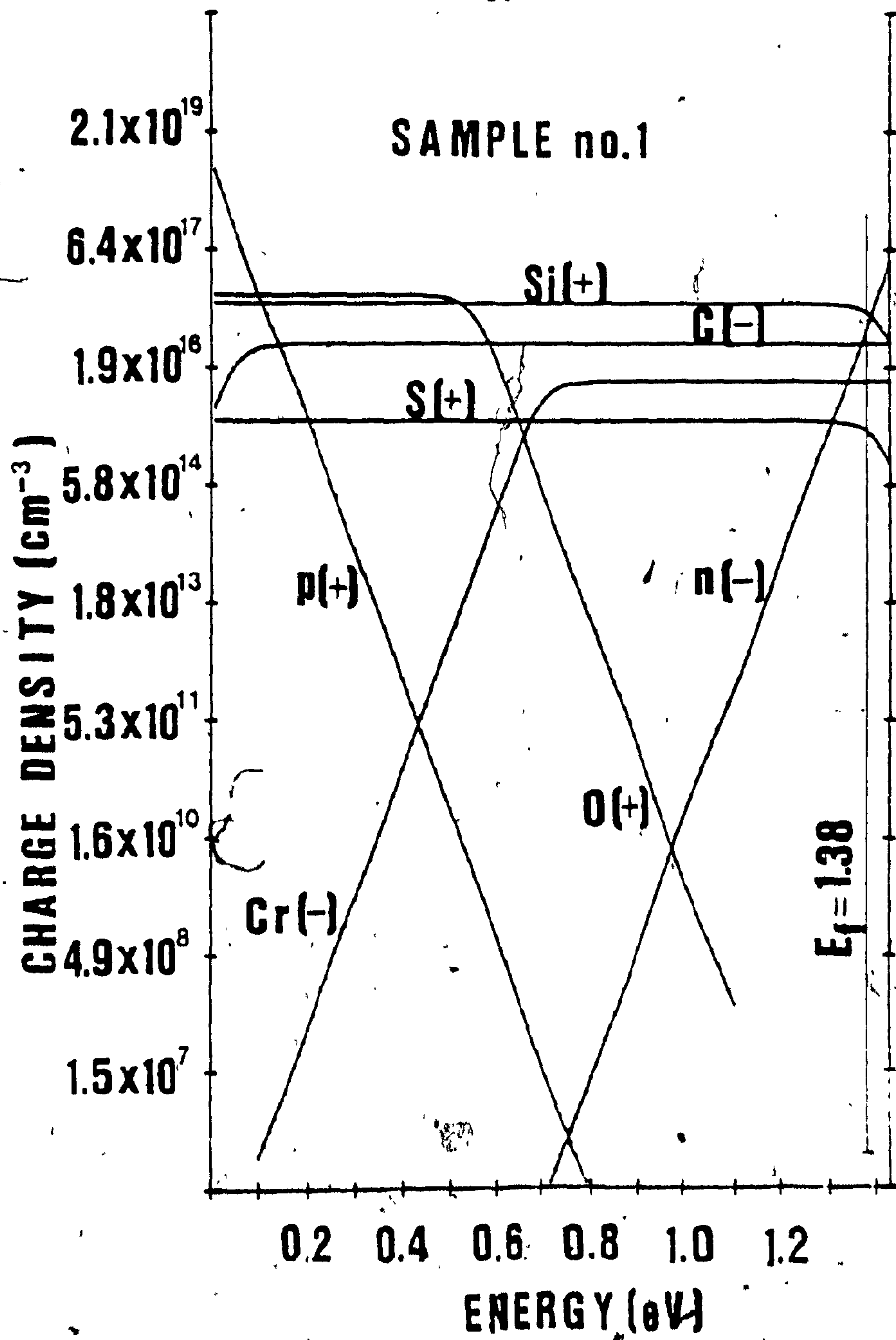

Fig. 4·6

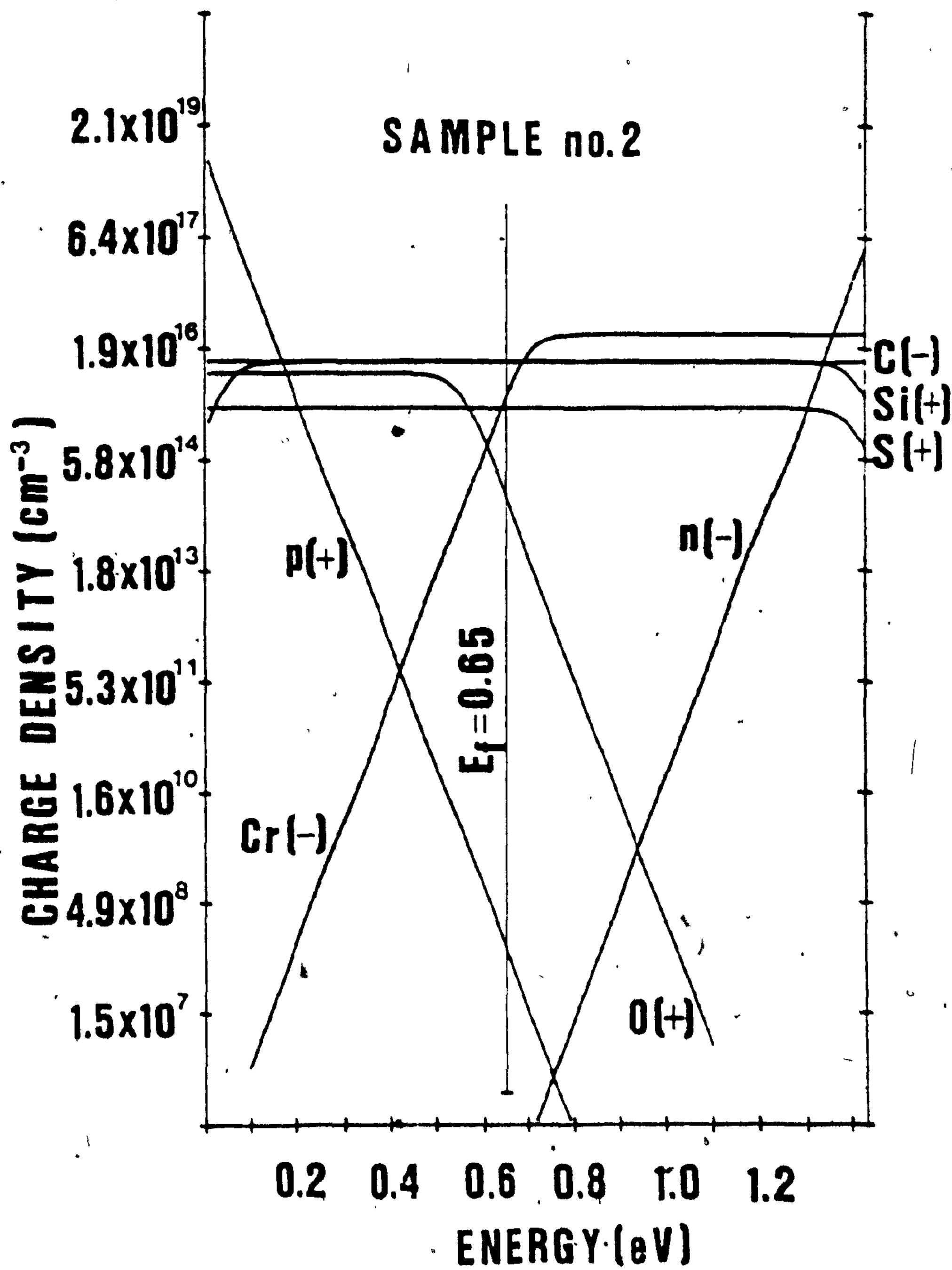

Fig. 4.7

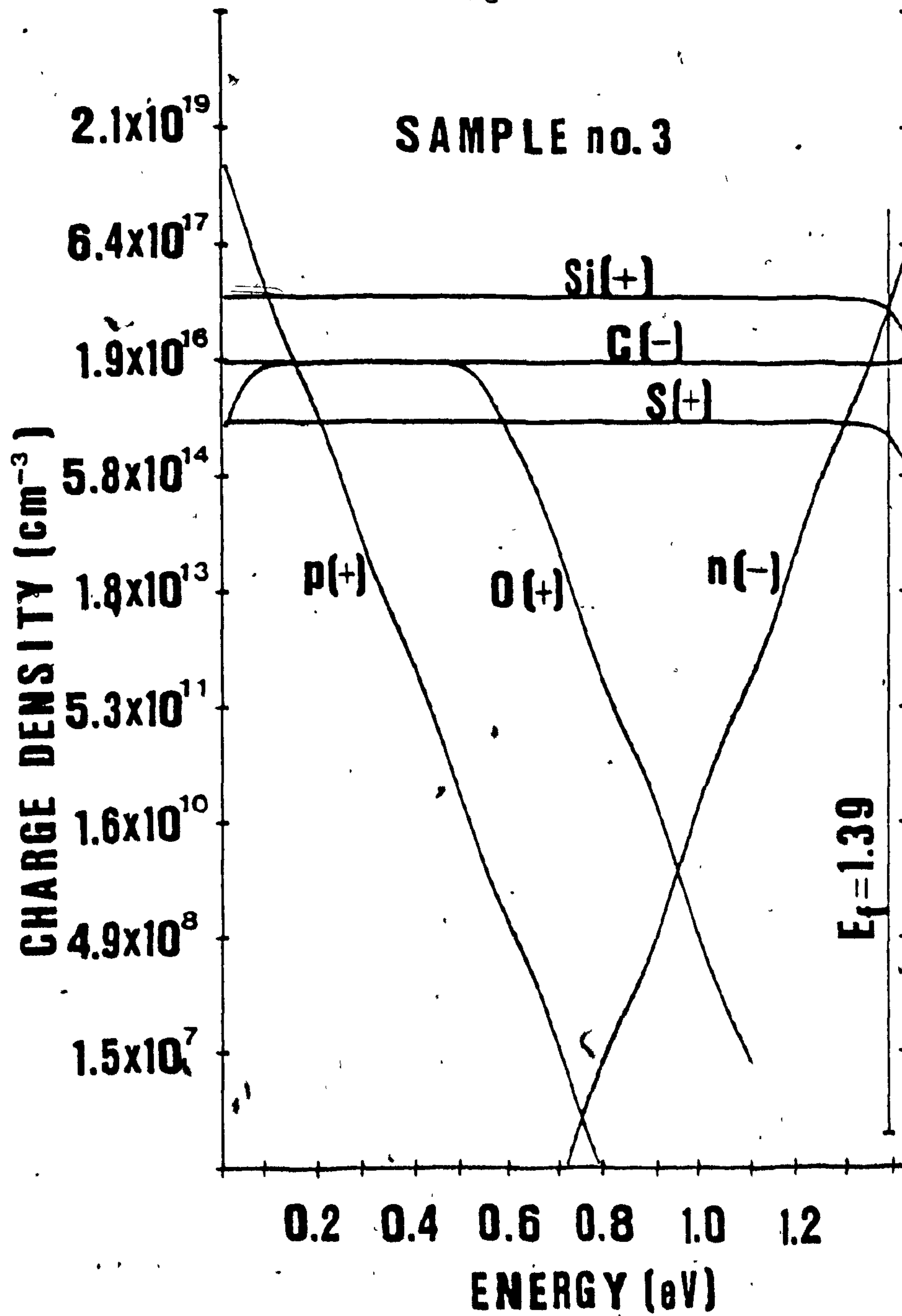

Fig - 4.8

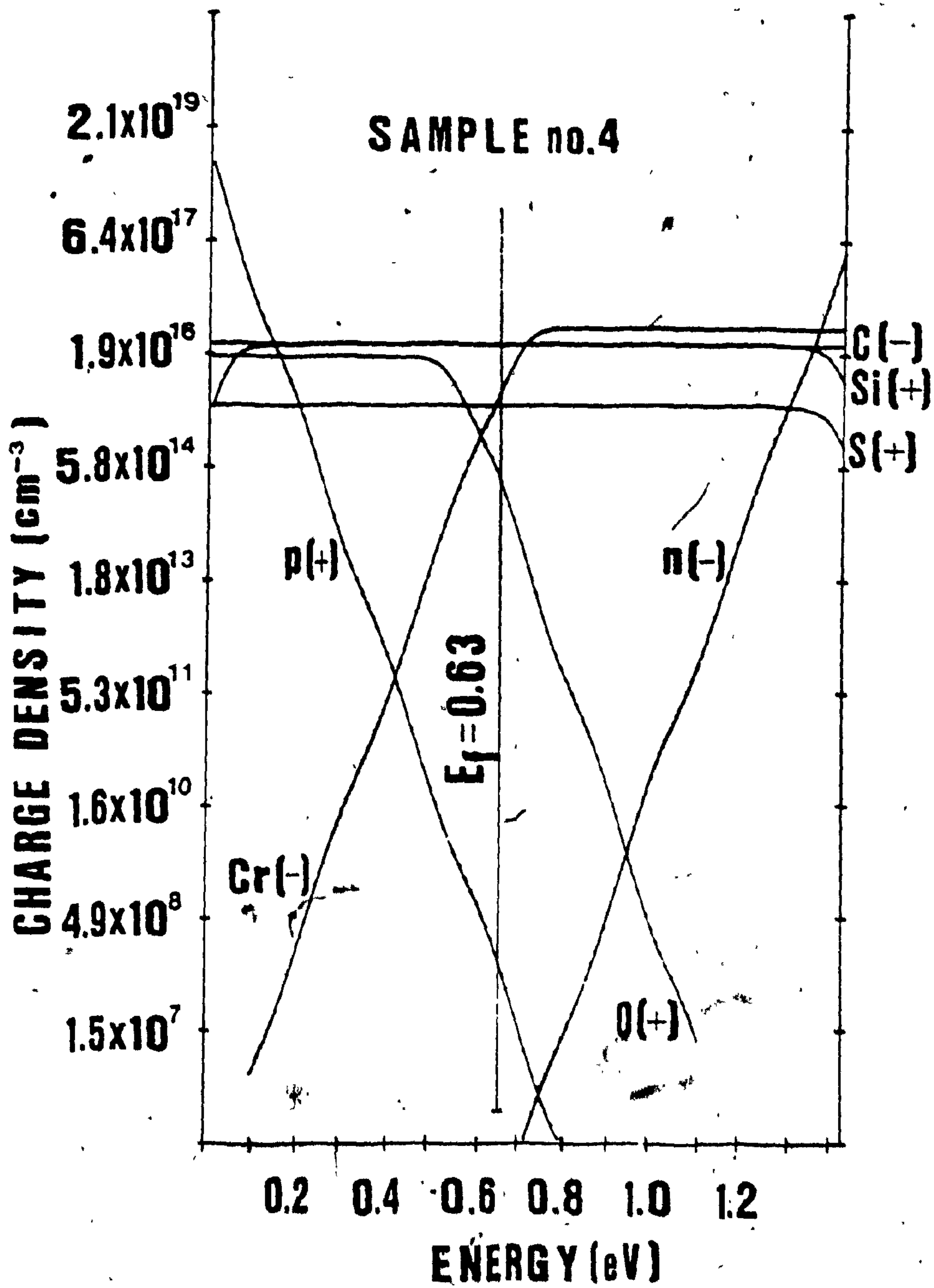

Fig. 4.9

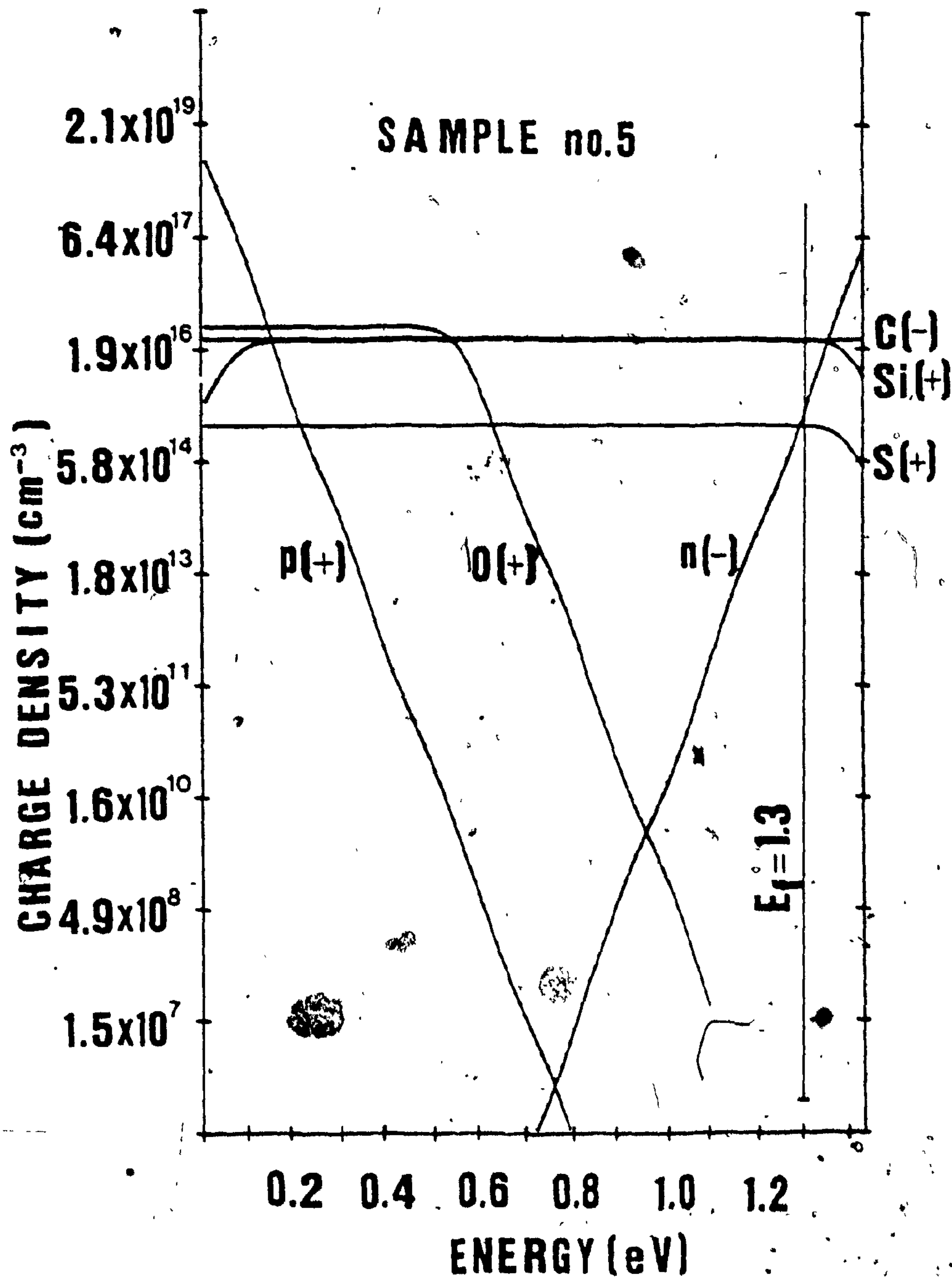

Fig. 4.10 Typical curves of $\ln(R_H e T^{3/2})^{-1}$ as a function of reciprocal temperature of semi-insulating GaAs samples based on the measured data collected in Table 4.3. (■) sample 2; (▲) sample 7; (●) sample 8.

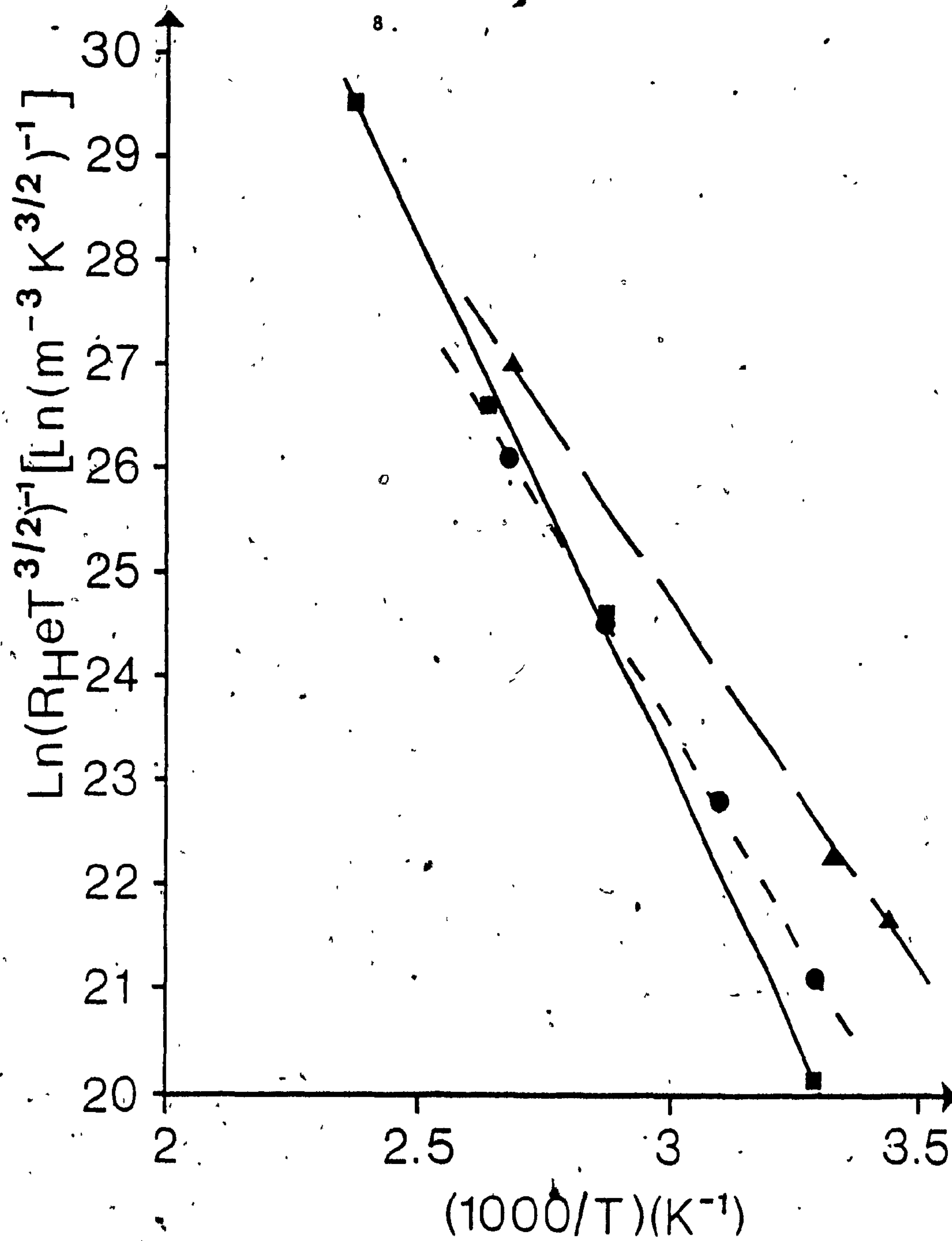

CHAPTER 5

SUMMARY AND CONCLUSION

A heat pipe assisted zone melter was developed to synthesize and grow large diameter (up to 55 mm) single crystals of GaAs. The placement of a heat pipe at the end of the ampule created a dynamic temperature profile and facilitated the control of the arsenic reservoir temperature. This method of application prevented the exposure of the heat pipe to high temperatures and extended its life indefinitely.

The narrow hot zone prevented the sagging and deformation of the ampule and reduced the diffusion of impurities from the ampule. In effect, the combination of zone melting and heat pipe assisted control enables the precise control of stoichiometry, improves purity, and removes restrictions on size of crystal due to the sagging of the ampule.

A multi level model for the calculation of the position of the Fermi level was developed. The model takes into consideration all the impurities indicated by the MSA.

The semiconducting or semi-insulating character of GaAs was determined by the position of the Fermi level. The resulting calculated transport properties were compared with the measured Hall coefficients and resistivities. The calculated and measured semiconducting and semi-insulating characters of all the crystals were in agreement. In all cases, the measured and calculated Hall coefficients and resistivities indicate excess n-type character. A possible source of the excess

donors was attributed to the phase extent of GaAs, since all the crystals were grown with a slight arsenic overpressure.

REFERENCES

1.1 S.M. Sze, In Physics of Semiconductor Devices, Wiley, New York, 1969, p. 57.

2.1 L.R. Weisberg, F.D. Rosi, and P.G. Herkart, "Properties of Elemental and Compound Semiconductors", Metallurgical Society Conference, Vol. 5, Interscience Publishers, Inc., New York, 1960.

2.2 J.L. Richards, J. Applied Physics, 31, 600, 1976.

2.3 R. Gremmelmaier, Z. Naturforsch, 11a, 511, 1956.

2.4 T.R. Aucoin, M.J. Wade, R.L. Ross and R.O. Savage, Solid State Technology, 22, 1979, 59.

2.5 J.M. Parsey, Y. Nanishi, J. Lagowski, and H.C. Gatos, J. Electrochemical Society, 129, 389, 1982.

2.6 W.G. Pfann, Trans, AIME, 194, 747, 1952.

2.7 A. Steinemann and U. Zimmerli, Solid State Electronics, 6, 597, 1963.

2.8 A. Lin, Ph.D. Thesis, Stanford University, 1975, Elec. Eng.

2.9 M. MacSkayls, Phys. Stat. Sol., (a), 17, 497, 1973.

2.10 D.L. Kendall, "Diffusion", Semiconductors and Semimetals, Vol. 4, Academic Press, New York, 1968, p. 163.

2.11 G.R. Cronin and R.W. Haisty, J. Electrochemical Society, 111, 874, 1964.

2.12 D.C. Look, J. Electronic Materials, 7, 1, 1978.

2.13 A.L. Lin and R.H. Bube, J. Appl. Phys., 47, 1859, 1976.

2.14 A. Lang, Phys. Rev. B., 15, 989, 1977.

2.15 K. Kitahara, K. Nakai, A. Shibatomi, and S. Ohkawa, J. Appl. Phys., 50, 5339, 1979.

2.16 D.C. Look, Solid State Commun., 24, 825, 1977.

2.17 R. Zucca, In Semi-insulating III-V Materials Conference, Institute of Physics, London SW1X8QX, University of Nottingham, 1980, p. 105.

2.18 P.F. Linquist, J. Appl. Phys., 48, 1262, 1977.

3.1 P. Hartman, Crystal Growth: An Introduction, North Holland, Amsterdam, 1973, p. 467.

3.2 J. Steininger and T.B. Reed, J. Crystal Growth, 13/14, 1972, 106.

3.3 K.T. Feldman and G.H. Whiting, Mech. Eng., 89 (2), 1967, 30.

3.4 Atlas, Stainless Steels Technical Data.

3.5 J.E. Kemme, "Heat Pipe Capability Experiments", report L.A. 3585-MS, UC-34, TID 4500.

3.6 N. Yemenidjian and B.A. Lombos, J. Crystal Growth, 56, 1982, 163.

3.7 L. Ekstrom and L.R. Weisberg, J. Electrochemical Society, 109, 321, 1962.

4.1 Spark Source Mass Spectrographic Analyses was performed at the National Research Council Analytical Chemistry Division in Ottawa by Dr. D.S. Russel.

4.2 R.N. Thomas, H.M. Hobgood, G.W. Eldridge, D.L. Barrett and T.T. Braggins, Solid-State Electronics, Vol. 24, 1981, pp. 387-399.

4.3 C.G. Hopkins, V.R. Deline, R.J. Blattner, and C.A. Evans, Jr., Appl. Phys. Lett., 36 (12), 15 June 1980, pp. 989-990.

4.4 M.S. Abrahams and E.S. Buiocchi, J. Appl. Phys., 36, 2855, 1965.

4.5 L.I. Greene, J. Appl. Phys., 48, 3739, 1977.

4.6 J.M. Parsey Jr., Y. Nanishi, J. Lagowski and H.C. Gatos, J. Electrochemical Society, 128, 936, 1981.

4.7 ANSI/ASTM F76-73, pp. 359.

4.8 M. Wittmer, R. Pretorius, J.W. Mayer and M.A. Nicolet, Solid State Electr., 20, 433, 1977.

4.9 B.A. Lombos, N. Yemenidjian and M. Averous, Canadian Journal of Physics, 60, 35, 1982.

4.10 Y.P. Varshni, Physica, 34, 149, 1967.

4.11 S.M. Sze, Physics of Semiconductor Devices, Wiley, New York, 1969, pp. 57.

4.12 R. Zucca, J. Appl. Phys., 48, 1987, 1977.

4.13 G.M. Martin, J.P. Farges, G. Jacobi and J.F. Hallais, J. Appl. Phys., 51, 2840, 1980.

4.14 C. Fau, M. Averous, J. Calas and B.A. Lombos, Can. J. Phys., 56, 610, 1978.

4.15 W. Schockley, Electrons and Holes in Semiconductors, D. Van Nostrand Co., Inc., New York, 1950, p. 466.

4.16 S.M. Sze, Physics of Semiconductor Devices, Wiley, New York, 1969, pp. 30.

4.17 A.L. Lin, E. Omelianovski, and R.H. Bube, J. Appl. Phys., 47, 1852, 1976.

4.18 G.M. Martin, A. Mitonneau and A. Mircea, Electron. Lett., 13, 191, 1977.

4.19 R.G. Chambers, Proc. Phys. Soc., A, 1952, 65, 903.

4.20 D.L. Rode, Phys. Status Solidi, 55, 687, 1973.

4.21 R.A. Smith, Semiconductors, 2nd Ed., Cambridge University Press, 1978.

4.22 J.A. Van Vechten, J. Electrom. Soc., Vol. 122, 423, 1975.

4.23 M.E. Straumanis and C.D. Kim, Acta Crystallogr., 19, 256, 1965.

4.24 J. Lagowski, H.C. Gatos, J.M. Parsey, K. Wada, M. Kaminska and W. Walukiewicz, Appl. Phys. Lett. 40 (4), 342, 1982.

4.25 D.E. Holmes, R.T. Chen, K.R. Elliot and C.G. Kirkpatrick, Appl. Phys. Lett., 40, 46, 1982.

4.26 S.M. Sze, Physics of Semiconductor Devices, Wiley, New York, 1969, p. 40.

APPENDIX A

Considering equation [4.1], the terms on the left hand side (LHS) represent the intrinsic electrons and the sum of the ionized acceptors. The terms on the right hand side (RHS) represent the intrinsic holes and the sum of the ionized donors.

Equations [4.2] and [4.3] allow us to calculate the intrinsic carriers as a function of the energy gap and the Fermi level. Similarly, the ionized impurity concentrations N_{ai}^{-} and N_{dj}^{+} are related to their chemical concentrations by equations [4.5] and [4.6].

The chemical concentrations of the various impurities N_{ai} and N_{dj} are indicated by the MSA, their respective ionization potentials E_{ai} and E_{dj} are obtained from previously published references.

The energy gap E_g for a given temperature is calculated from equation [4.4].

Since the Fermi level lies within the energy gap and by assuming that the Fermi level is several KT away from the band edges (hence Maxwell Boltzmann statistics apply), it is possible to calculate all the terms of equation [4.1] for any E_f. If the value of E_f is too small; then, the RHS of equation [4.1] will be larger than the LHS. Conversely, if the chosen value of E_f is too large, then the LHS will be larger than the RHS.

By iterating the value of E_f from .1 to E_g, the LHS and RSH of equation [4.1] are calculated. The particular value of E_f for which

the LHS of equation [4.1] equals the RHS gives the correct value of the Fermi level.

In the following computer program written in "Basic", variable S1 = N1 + N2 + N4 represents the LHS of equation [4.1]

where N1 = ionized carbon concentration

N2 = ionized chrome concentration

N4 = intrinsic donor concentration

variable S2 = N3 + N5 + N6 + N7 represents the RHS of equation [4.1]

where N3 = ionized oxygen concentration

N6 = ionized silicon concentration

N7 = ionized sulphur concentration

N5 = intrinsic hole concentration

Once the correct value of E_f is determined, the electron and hole concentrations are calculated from equations [4.2] and [4.3], and printed. The electron and hole mobilities μ_n and μ_p corresponding to the calculated carrier concentrations are obtained from published references and entered as data. The conductivity and Hall coefficient are then calculated.

The same results can be obtained graphically as illustrated in Figures 4.6-4.9. Variables N1, N2, N4 are plotted as a function of E_f, and subsequently their sum S1 is plotted corresponding to the LHS of equation [4.1] as a function of E_f (not shown).

Similarly, variables N3, N5, N6, N7, are plotted as a function of E_f, and subsequently their sum S2 is plotted corresponding to the RHS of equation [4.1] as a function of E_f (not shown).

The intersection of curves S1 and S2 yields the correct value of E_f, i.e., equal numbers of ionized donors and acceptors.

COMPUTER PROGRAM TO CALCULATE AND PLOT FERMI LEVEL

```
10    DISP "GIVE THE CONCENTRATIONS"
20    WAIT 2000
30    DISP "CARBON CONC. = ??? (CM↑(-3))"
40    WAIT 2000
50    INPUT C1
60    DISP "CHROMIUM CONC. = ??? (CM↑(-3))"
70    WAIT 2000
80    INPUT C2
90    DISP "OXYGEN CONC. = ??? (CM↑(-3))"
100   WAIT 2000
110   INPUT C3
120   DISP "SILICON CONC. = ???(CM↑(-3))"
130   WAIT 2000
140   INPUT C6
150   DISP "SULPHUR CONC. = ??? (CM↑(-3))"
160   WAIT 2000
170   INPUT C7
180   DISP "SAMPLE #=??"
190   WAIT 2000
200   INPUT S
210   PRINT "SAMPLE #="S
220   PRINT " CARBON CONC.="C1"(CM↑(-3))"
230   PRINT "CHROMIUM CONC.= "C2"(CM↑(-3))"
240   PRINT "OXYGEN CONC.="C3"(CM↑(-3))"
250   PRINT "SILICON CONC.="C6"(CM↑(-3))"
260   PRINT "SULPHUR CONC.="C7"(CM↑(-3))"
270   SCALE -0.5, 2,9,48
280   DISP"T=??? IN (K)"
290   WAIT 2000
300   INPUT T
310   V=(1.43+(300-T)*3.4E-04)
320   PRINT "T="T"(K)"
330   PRINT "EG="V"(EV)"
340   XAXIS 13,0.1,0,V
350   YAXIS 0,3,5,13,48
360   YAXIS V,3,5,13,48
370   PLOT 0,13,+1
380   CPLOT +10,-4
390   GOTO 420
400   LABEL (490,1.7,1.7,0,10/10)
410   LABEL(*)"       ENERGY (EV)"
420   FOR X = 0.2 TO 1.2 STEP 0.2
430   PLOT X,11,1
440   CPLOT -2.3,0
450   GOTO 610
460   LABEL (470)X
470   FORMAT F4.1
```

```
480  NEXT X
490  FORMAT E8.1
500  LABEL (490,1.5,1.7,0,10/10)
510  FOR Y=13 TO 44.5 STEP 3.5
520  IF Y=13 THEN 570
530  PLOT 0,Y,1
540  CPLOT -10.0
550  Z=EXP(Y)
560  LABEL (490)Z
570  NEXT Y
580  PLOT 0,13
590  CPLOT -12,4
600  LABEL(*,1.7,1.7,PI/2,10/10)"            CHARGE DENSITY (CM↑(-3))"
610  K=8.617E-05
620  LABEL(*,1.5,1.7,0,10/10)
630  IF C1<1E+07 THEN 740
640  FOR X=0.01 TO V STEP 0.01
650  N1=C1*(1-1/(1+(1/4)*EXP((X-0.019)/(K*T))))
660  Y=LOG(N1)
670  IF Y<13 THEN 700
680  PLOT X,Y
690  NEXT X
700  CPLOT 2,0
710  GOTO 730
720  LABEL (*)"C(-)"
730  IF C2<1E+07 THEN 840
740  FOR X=0.1 TO V STEP 0.01
750  N2=C2*(1-1/(1+(1/2)*EXP((X-).68)/(K*T))))
760  Y=LOGN2
770  IF Y<13 THEN 800
780  PLOT X,Y
790  NEXT X
800  CPLOT 2,-1
810  GOTO 830
820  LABEL (*)"CR(-)"
830  IF C3<1E+07 THEN 930
840  FOR X=0.01 TO 1.1 STEP 0.01
850  NC=C3*(1-1/(1+1/2)*EXP((V-0.86-X)/(K*T))))
860  Y=LOG(N3)
870  IF Y<13 THEN 900
880  PLOT X,Y
890  NEXT X
900  CPLOT +1,0
910  GOTO 930
920  LABEL(*)"O(+)"
930  FOR X=V TO 0.1 STEP -0.01
940  N4=8.5645161E+13*T↑(3/2)*EXP((X-V)/(K*T))
950  Y=LOG(N4)
960  IF Y<13 THEN 990
970  PLOT X,Y
980  NEXT X
990  CPLOT +4, +2
```

```
1000   GOTO 1020
1010   LABEL (*)"N(-)"
1020   FOR X=0.01 TO V STEP 0.01
1030   N5=1.9084085E+15*T↑(3/2)*EXP((-X)/(K*T)
1040   Y=LOG(N5)
1050   IF Y<13 THEN 1080
1060   PLOT X,Y
1070   NEXT X
1080   CPLOT -6,+2
1090   GOTO 1110
1100   LABEL (*) "P(+)"
1110   IF C6 1E+07 THEN 1220
1120   FOR X=0.01 TO V STEP 0.01
1130   N6=C6*(1-1/(1+(1/2)*EXP((V-0.002-X)/(K*T))))
1140   Y=LOG(N6)
1150   IF Y<13 THEN 1180
1160   PLOT X,Y
1170   NEXT X
1180   CPLOT 2, +1
1190   GOTO 1210
1200   LABEL (*) "SI(+)"
1210   IF C7<1E+07 THEN 1310
1220   FOR X=0.01 TO V STEP 0.01
1230   N7=C7*(1-1/(1+(1/2)*EXP((V-0.006-X)/(K*T))))
1240   Y=LOG(N7)
1250   IF Y<13 THEN 1280
1260   PLOT X,Y
1270   NEXT X
1280   CPLOT 2, -1
1290   GOTO 1310
1300   LABEL(*)"S(+)"
1310   FOR X=0.1 TO 1.4 STEP 0.01
1320   N1=C1*(1-1/(1+(1/4)*EXP((X-0.019)/(K*T))))
1330   N2=C2*(1-1/(1+(1/2)*EXP((X-0.68)/(K*T))))
1340   N3=C3*(1-1/(+1(1/2)*EXP((V-0.86-X)/(K*T))))
1350   N4=8.5645161E+13*T↑(3/2)*EXP((X-V)/(K*T))
1360   N5=1.9084085E+15*T↑3/2)*EXP((-X)/(K*T))
1370   N6=C6*(1-1/(1+(1/2)*EXP((V-0.002-X)/(K*T))))
1380   N7=C7*(1-1/(1+(1/2)*EXP((V-0.006-X)/(K*T))))
1390   S1=N1+N2+N4
1400   S2=N3+N5+N6+N7
1410   D1=S1-S2
1420   IF D1>0 THEN 1440
1430   NEXT X
1440   YAXIS X,30,14,42
1450   PLOT X,13
1460   CPLOT -1,10
1470   GOTO 1490
1480   LABEL(*,1.5,1.7,PI/2,10/10)"EF="X"(EV)"
1490   WRITE(15,490)"(C-)="N1"(CR-)="N2"(O+)="N3
1500   PRINT
```

```
1510  WRITE (15,490)"(N-)="N4"(P+)="N5
1520  WRITE (15,490)"(SI+)="N6"(S+)="N7
1530  PRINT
1540  PRINT "S1="S1"S2="S2
1550  H=1.60216E-19
1560  R1=-(H*N4)↑(-1)
1570  R2=(H*N5)↑(-1)
1580  DISP "ELECTRON MOBILITY = ??? (M↑2/(VOLT-SEC))"
1590  WAIT 2000
1600  INPUT UN
1610  DISP "HOLE MOBILITY = ??? (M↑2/VOLT-SEC))"
1620  WAIT 2000
1630  INPUT UP
1640  C1=N4*H*UN
1650  C2=N5*H*UP
1660  Z=1/(C1+C2)
1670  R3=(R1*C1*C1+R2*C2*C2)/(C1+C2)↑(2)*(1-18)
1680  WRITE (15,1650)Z
1690  WRITE (15,1660)R3
1700  WRITE (15,1670)X
1710  FORMAT 5X, "RESISTIVITY=,E15.4,"(OHM-CM)"
1720  FORMAT 5X,"HALL COEFFICIENT=",E15.4,5X,"(CM↑3/C)"
1730  FORMAT 5X,"FERMI ENERGY"=",E15.4,5X,"(EV)"
1740  GOTO 1840
1750  LABEL (490,1.5,1.7,0,10/10)
1760  PLOT 0,48,1
1770  CPLOT +10,0
1780  LABEL(*) "SAMPLE #"S
1790  PLOT 0,48,1
1800  CPLOT +10,-2
1810  LABEL (*)"T="T"(K)"
1820  PLOT 0,48,1
1830  CPLOT +10,-3.5
1840  FORMAT "RH=",E8.1,"(CM↑(3)/C)"
1850  LABEL (1780) R3
1860  PLOT 0,48,1
1870  CPLOT +10,-5
1880  OFRMAT "R=",E8.1,"(OHM-CM)"
1890  LABEL (1820)Z
1900  DISP "CONTINU=? YES:1, NO:0"
1910  WAIT 2000
1920  INPUT J
1930  IF J=1 THEN 280
1940  END
```